nagra.

Arbeitsbericht NAB 22-43

Bentonite Pore Waters (BPW) for SGT-E3:

Model Development, Testing and Final Calculations

January 2023

E. Curti

National Cooperative
for the Disposal of
Radioactive Waste

Hardstrasse 73
P.O. Box
5430 Wettingen
Switzerland
Tel. +41 56 437 11 11

www.nagra.ch

nagra.

Arbeitsbericht NAB 22-43

Bentonite Pore Waters (BPW) for SGT-E3:

Model Development, Testing and Final Calculations

January 2023

E. Curti

Paul Scherrer Institut

KEYWORDS

Bentonite pore water

National Cooperative
for the Disposal of
Radioactive Waste

Hardstrasse 73
P.O. Box
5430 Wettingen
Switzerland
Tel. +41 56 437 11 11

www.nagra.ch

Nagra Arbeitsberichte ("Working Reports") present the results of work in progress that have not necessarily been subject to a comprehensive review. They are intended to provide rapid dissemination of current information.
This report was prepared on behalf of Nagra. The viewpoints presented and conclusions reached are those of the author(s) and do not necessarily represent those of Nagra.

Table of Contents

List of Tables II

List of Figures III

1 Introduction 1

2 Model development 5
2.1 Short description of BPW model components 5
2.2 Detailed model description 6
2.2.1 Definition of Opalinus Clay input water 6
2.2.2 Implementation of Specific Ion interaction Theory (SIT) 7
2.2.3 Definition and selection of selectivity coefficients for cation exchange 10
2.2.4 Initial state of bentonite 11
2.2.5 Definition of Solid/Water (S/W) ratio based on anion porosity 13
2.3 Model implementation in GEM-Selektor 17
2.3.1 Definition of GEM-Selektor input 17
2.3.2 Brief description of GEM-Selektor output 21

3 BPW calculations: model testing (TDB 12/07) 25
3.1 Database and parameter variations 25
3.1.1 Database, activity model and treatment of minerals 25
3.1.2 Parameter variations 26
3.2 Discussion of BPW calculations 27
3.2.1 Source case 27
3.2.2 Effect of surface hydroxyl groups (= SOH) and pH buffering 29
3.2.3 Effect of bentonite compaction (“porosity”) 32
3.2.4 Effect of unconstrained pCO_2 (closed system) 35
3.2.5 Effect of different fixed pCO_2 37
3.2.6 Control of oxidation potential (Eh) through iron phases 40
3.2.7 Chemical evolution of the bentonite pore water 43

4 Final BPW calculations (TDB 2020) 49
4.1 Transfer of model to TDB 2020 49
4.2 Definition of Opalinus Clay Waters (OPAw) 49
4.3 Calculation of Bentonite Pore Waters (BPW) 52

5 Acknowledgments 57

6 References 59

App. A List of SIT coefficients used in BPW calculations A-1

App. B Conversion of Gaines-Thomas to Vanselow selectivity coefficients B-1

App. C Explanation of discrepant Fe concentrations in calculated Opalinus Clay waters C-1

List of Tables

Tab. 2-1: Composition and characteristics of provisional Opalinus Clay pore waters as defined at Uni Bern, based on analyses from Bülach borehole samples aqueous extracts 6

Tab. 2-2: Recalculations of ACW-3 Opalinus Clay pore water from Uni Bern (column 1) using GEM-Selektor and PSI-Nagra thermodynamic database (v. 1207) applying seven different aqueous activity models 8

Tab. 2-3: Equations describing the various activity models tested on OPAw 9

Tab. 2-4: Primary Gaines-Thomas (K_G) and converted Vanselow (K_V) selectivity coefficients for aqueous solution-MX80 bentonite exchange used in the BPW model 11

Tab. 2-5: Initial state of MX-80 bentonite used as reactant material in the calculation of BPW composition 12

Tab. 2-6: Total porosity, maximum anion accessible porosity and anion accessible porosity at I = 0.61 m for 3 different degrees of compaction of MX-80 bentonite 14

Tab. 2-7: Determination of OPAw input amounts and corresponding S/W ratios from eqs. (9) and (10) for three different degrees of compaction 21

Tab. 3-1: Overview of BPW calculations 26

Tab. 3-2: Results of source case BPW calculations 27

Tab. 3-3: Results of BPW calculations: effect of surface hydroxyl speciation 30

Tab. 3-4: Results of BPW calculations: effect of bentonite compaction 33

Tab. 3-5: Results of BPW calculations: effect of unconstrained pCO_2 35

Tab. 3-6: Results of BPW sequential reactor calculations (ρ_{dry} = 1'450 kg m^{-3} and closed system) after 1 and 1'000 water exchange cycle 46

Tab. 4-1: Opalinus Clay in-situ pore waters from the NL-ZNO regions: original compositions from Bern University (BU) compared to compositions adjusted using GEM-Selektor at PSI 50

Tab. 4-2: Opalinus Clay in-situ pore water from the Bülach-1 borehole and two artificial low-salinity and high salinity pore waters derived from OPAw_NL-ZNO-22 51

Tab. 4-3: Upper section: in-situ bentonite pore waters (BPW) for the NL-ZNO region compared to the reacting Opalinus Clay Waters (OPAw) 53

Tab. 4-4: Upper section: in-situ Bülach bentonite pore water (BPW_BUL-28) compared to the reacting OPAw and artificial low-salinity and high-salinity BPWs 55

Tab. A-1: Selected SIT coefficients for BPW chemical modelling A-1

Tab. B-1: Transformation of Gaines-Thomas to Vanselow selectivity coefficients from eq. (A2-8b) for Na^+-K^+, Na^+-Mg^{2+}, Na^+-Ca^{2+}, Na^+-Sr^{2+} and Na^+-Ba^{2+} exchange reactions B-4

Tab. C-1: Comparison of results obtained for the low pCO_2 variant of the ZNO Opalinus Clay pore water C-1

Tab. C-2: Comparison of saturation indices of iron minerals in three variants of the Opalinus Clay pore water OPAw-ZNO-28 ..... C-3

List of Figures

Fig. 2-1: Schematic view of the BPW model construction 5

Fig. 2-2: Anion accessible porosities as function of ionic strength for MX-80 bentonite with 3 different degrees of compaction. The vertical broken line marks the approximate ionic strength of calculated BPW (I = 0.6 m, see later) 15

Fig. 2-3: Volumetric distribution of water types and solid in compacted bentonite for three different dry bulk densities 16

Fig. 2-4: COMPOS entry for provisional Bülach water ACW3a, used as reacting water in the BPW calculations 17

Fig. 2-5: GEM-Selektor input specification of montmorillonite for 1 kg of MX-80 bentonite 18

Fig. 2-6: Typical recipe input window for BPW model calculations. The specified units (M) are moles for all species except the COMPOS ACW3_ext and MX80_exch, for which 1 M corresponds exactly to 1 kg of aqueous solution and 1 kg of dry MX-80 bentonite, respectively 19

Fig. 2-7: GEM-Selektor screenshot after successful BPW calculation 22

Fig. 2-8: Screenshot of GEM-Selektor BPW output file (example calculation) 23

Fig. 3-1: Eh-pH diagrams for BPW conditions at 25 °C and 1 bar 42

Fig. 3-2: Principle of sequential reactor provided in the GEM2MT module as applied to the BPW evolution 43

Fig. 3-3: Calculated evolution of BPW as a function of water exchange cycles at the external interface of MX80 bentonite 45

Fig. B-1: Ratio of Gaines-Thomas to Vanselow constant as a function of equivalent fraction and charge of the exchanging cations (binary system) B-3

1 Introduction

In the framework of the Sectoral Plan for Deep Geological Repositories, stage 3 ("Sachplan Geologische Tiefenlager", Phase 3, shortly SGT-3) PSI was in charge to derive composition and chemical characteristics of pore waters in equilibrium with compacted bentonite under the conditions expected in the planned HLW/SF repository. These pore waters are a pre-requisite to derive solubility limits and sorption coefficients (K_D) of dose-relevant radionuclides for safety assessment calculations. These NAB is a summary of TM-44-21-02 Rev. 1 authored by E. Curti. In the TM, additional information for the model setup are presented.

Bentonite pore waters were defined for the three preceding Swiss safety assessments Kristallin-I, Entsorgungsnachweis and SGT-2 (Curti 1993, Curti & Wersin 2002, Bradbury et al. 2014) reflecting the specificity of host-rock type (crystalline basement rocks or Opalinus Clay), available underground water data and the evolution of concepts used to model the interaction between aqueous solutions and compacted clay. This report presents in detail the development of an updated thermodynamic model to derive Bentonite Pore Waters (BPWs) for SGT-3. Moreover, a comparison is made with other approaches and previous BPW models. Finally, preliminary pore water calculations based on provisional water input data derived from the at that time ongoing drilling program were carried out using GEM-Selektor v. 3.7 with the PSI-Nagra database v. 12/07 and discussed.

To date, there is no consensus on a scientifically sound approach on how to model aqueous solutions in equilibrium with compacted clay. This is mainly due to the intrinsic difficulties in measuring in-situ properties and in unravelling the complex nature of water/clay interactions under narrow confinement. For instance, an important proportion of water saturating compacted bentonite enters the interlayer space of montmorillonite, where exchangeable cations reside. In all but the first BPW model applied so far (Kristallin-I), interlayer water was considered to be unreactive and thus excluded from equilibrium calculations. This implies that only the external interparticle water is considered to be able to undergo complexation or dissolution/precipitation reactions. Even more importantly, due to the high degree of compaction and the negatively charged surface of the clay, interparticle water splits into two significant fractions:

a) Water associated to the electrical diffuse double layer (DDL) characterized by a charge-compensating cation excess and anion exclusion.

b) "Free" electrically neutral water, the volume of which is defined by the so-called anion porosity.

Classical aqueous chemistry involving complexation and dissolution/precipitation reactions can be safely applied only in electrically neutral "free" water. The inclusion of DDL water in the equilibrium calculations always involves simplifying assumptions and approximations (see e.g. Wersin et al. 2004). Because the relative volumes of the aforementioned three types of water depend on electrolyte concentration (ionic strength) and clay compaction (dry density), and because the salinity of the interparticle water may be affected by the nature of the bentonite resaturation process[1], one is faced to the non-trivial problem of defining volume and composition of reactive water. The relative volumes of DDL and free water may even vary during an equilibration step, e.g. due to precipitation reactions which tend to reduce both ionic strength and porosity.

[1] If interlayer water originates from the intruding aqueous solution, the resulting interparticle water will be more saline than the original intruding water. Alternatively, one may assume that slow water vapour adsorption contributes to partial or full interlayer saturation. In the latter case, the unreacted interparticle water will have the same composition as the intruding water.

In the BPW calculations developed for Kristallin-I (Curti 1993) and "Entsorgungsnachweis" (Curti & Wersin 2002), all water saturating bentonite (i.e. interlayer + external) was considered to be reactive. However, as a spin-off of the "Entsorgungsnachweis" safety assessment this issue was discussed and a variant was calculated, in which complexation and dissolution/precipitation equilibria were limited only to the interparticle water (Wersin et al. 2004). Finally, for the definition of BPWs in the context of SGT-2, interlayer water was consistently excluded from the equilibrium calculations (Bradbury et al. 2014). In the two latter cases, it was assumed that the Opalinus Clay pore water (OPAw) reacts with bentonite pre-saturated via vapour adsorption, implying that the salinity of intruding OPAw does not increase due to uptake of pure water in the interlayer.

For SGT-2, two model variants were applied, denoted as "conventional" and "new" model. In the conventional model, montmorillonite was treated as a pure ion exchanger. Any dissolution or precipitation of montmorillonite was neglected. This (still customary) treatment is usually justified by the very low solubility of this mineral at low temperatures and by the absence of reliable thermodynamic data (solubility products) for montmorillonite. The "new" model (Berner et al. 2013, Bradbury et al. 2014) takes into account minor dissolution/precipitation of montmorillonite by calibrating thermodynamic data against in-house solution data from batch experiments. Moreover, an ill-defined soluble form of magnetite ("hydro-magnetite") was used in the "new" model, whereas in all "conventional" calculations the thermodynamic data for crystalline magnetite (those present in the PSI-Nagra database) was used. This choice has consequences on the calculated redox potential, as discussed later.

Finally, the "new" model calculates equilibrium without constraining carbon dioxide partial pressure (pCO_2) to a pre-defined fixed value. In the "conventional" model this parameter was fixed to values derived from borehole data. It is important to realize that these two alternatives reflect distinct assumptions on the mobility of dissolved CO_2 through the near-field. A constrained pCO_2 implicitly assumes fast diffusion and a permanent connection with a large external CO_2 reservoir in the geosphere. In contrast, leaving the pCO_2 unconstrained implies that the bentonite system is essentially treated as a closed system which equilibrates only internally and is completely separated from external CO_2 sources. The two approaches thus represent two limiting cases of an equilibration process that probably proceeds in reality in-between. The results of SGT-2 calculations nevertheless showed only minor differences in the results of these two limiting calculations, indicating that other powerful buffering mechanisms play a more important role in the system of interest.

The SGT-3 model developed here is in-line with the "conventional" variant of the SGT-2 approach, with a few conceptual and technical modifications that will be described later in this report. All (preliminary) calculations presented in this report simulate a one-cycle reaction at 25 °C and 1 bar total pressure between normative amounts of bentonite and interparticle water corresponding to a predefined compaction of the bentonite. As for SGT-2, variants with both constrained and unconstrained pCO_2 were calculated in order to assess the impact of the opposite assumptions on CO_2 diffusivity.

As an alternative to the aforementioned models (all treating equilibrium in compacted clays as interaction between distinct solid phases and a separated aqueous solution) models based on Donnan-type equilibria have been recently proposed and applied (Birgersson & Karnland 2009, Tournassat 2016, Gimmi & Alt-Epping 2018), in which the entire compacted clay-water system is treated thermodynamically as a single homogeneous phase. The debate on which type of model is scientifically sounder, is still ongoing (Birgersson 2017, Birgersson et al. 2017). However, Donnan treatments of compacted clays are so far limited to major electrolyte ions. No complete description of trace solutes (e.g. radionuclides) inside the saturated bentonite is currently available and therefore this approach is presently not applicable to safety assessment purposes.

Consequently, the classical and still customary modelling method involving separate aqueous and solid phases is used here.

No reactive transport calculations to determine the temporal and spatial evolution of the bentonite pore water system are presented in this study. Such calculations (focussed on the interaction of an external low-pH concrete with bentonite and Opalinus Clay) were extensively carried out in the framework of SGT-2 (Berner et al. 2013) and an update will be presented soon in a separate report. The calculations showed that the predicted modifications in exchanged cation distribution, mineralogy and porosity induced by the concrete liner will affect only a small part of the bentonite external boundary, leaving most of the backfill material intact. The conclusions drawn from that study are anticipated to be still valid and can be taken over for SGT-3.

2 Model development

2.1 Short description of BPW model components

The operational components of the BPW model are shown in the flow diagram of Fig. 2-1. The starting point were chemical analyses of Opalinus Clay aqueous extracts obtained during Nagra's borehole campaign for SGT-3, supplied by Bern university's water-rock interaction group (Mäder & Wersin 2022). After small adjustments (see Section 2.2.1) and application of different aqueous activity models, either using PhreeqC or GEM-Selektor speciation programs, eight slightly different Opalinus Clay water (OPAw) compositions, saturated with celestine, gypsum, calcite were obtained, all at equilibrium with the same CO_2 partial pressure. The tested activity models were Truesdell-Jones (TD), five variants of Debye-Hückel (DH-), Davies and the Specific Ion interaction Theory (SIT).

For the reasons described in Section 2.2.2 the SIT activity model, implemented in the GEM-Selektor code, was preferred and selected for the further development of the BPW model. The resulting water (OPAw PSI) proved to differ only slightly in composition, pH and ionic strength from the equivalent water defined at Bern's university (OPAw UniBe) using PhreeqC and Truesdell-Jones activity model. OPAw PSI was used as input in the later calculations to simulate reaction with MX-80 bentonite. The calculations assume a given initial Solid/Water (S/W) ratio and anion porosity (ε_{an}) and take into account available experimental information on the initial state of the bentonite (initial population of exchangeable interlayer sites, the initial state of protonation of surface hydroxyl groups on the edge of clay platelets (= SOH sites) and the inventories of minor minerals). The result is an equilibrium system consisting of bentonite pore water (BPW), a final exchanged ion population, a distribution of protonated and deprotonated surface sites and an assemblage of minor solids at equilibrium. The BPW calculations presented in this report include 11 elements: Al, C, K, H, K, Mg, Na, O, S, Si, Sr.

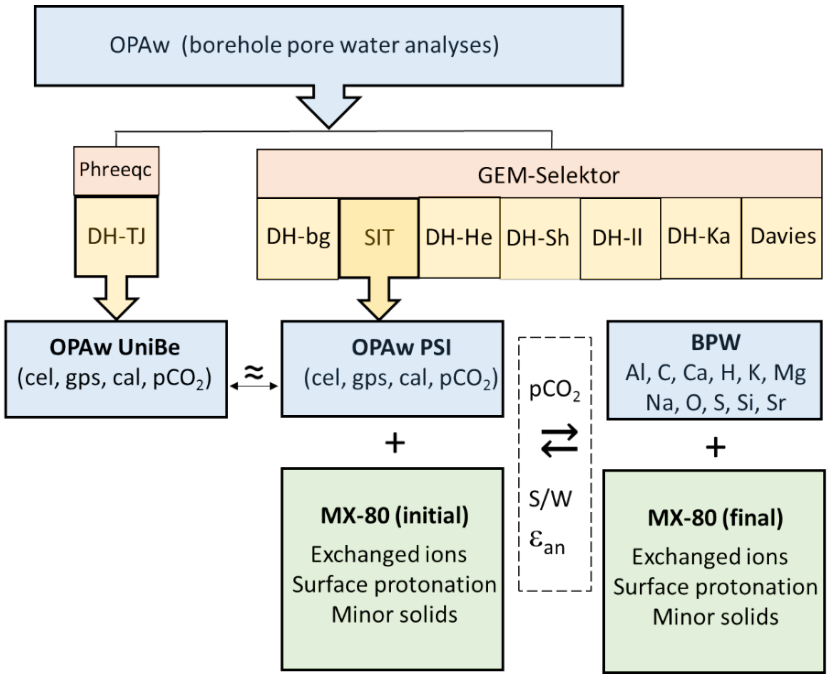

Fig. 2-1: Schematic view of the BPW model construction

2.2 Detailed model description

2.2.1 Definition of Opalinus Clay input water

For the development of the BPW model, the first available data from Bülach borehole were used, supplied by the water-rock interaction group at the Geological Institute of Bern University (documented in Mäder & Wersin 2022). After small corrections for temperature (from 23 °C to 25 °C) a slightly charge-misbalanced solution (+ 1.71%) was obtained (solution ACW-1, Tab. 2-1). Moreover, small deviations from perfect saturation appear with respect to common reactive minerals ubiquitous in the Opalinus Clay formation, notably celestine, gypsum and calcite.

Tab. 2-1: Composition and characteristics of provisional Opalinus Clay pore waters as defined at Uni Bern, based on analyses from Bülach borehole samples aqueous extracts[2]

	BUL1-474-AD **input** (chemical analysis) [mg/l]	**ACW-1** **output (#1)** [mol/kgw]	**ACW-3** **output (#2)** [mol/kgw]
pH, in-line	7.27		7.27
Temperature (°C)	23	25	25
Na	8088	3.62E-01	3.46E-01
K	73.3	1.93E-03	1.93E-03
Ca	1587	4.07E-02	3.88E-02
Mg	421	1.78E-02	1.78E-02
Sr	44.9	5.27E-04	3.37E-04
Cl	13995	4.06E-01	4.06E-01
Br	21.8	2.80E-04	
SO4	2783	2.98E-02	2.77E-02
C(4)	33.4	5.56E-04	8.02E-04
Si	5.77	9.92E-05	
DOC	708	5.27E-04	
a(H_2O)		0.986	0.986
ionic strength		5.18E-01	5.06E-01
total alkalinity [eq/kg]		5.33E-04	7.69E-04
charge imbalance		1.55E-02	0
%-imbalance		1.71	0
log_p(CO_2) [bar]		-2.99	-2.84

[2] These waters are preliminary water, which have been provided to PSI for the model development.

Tab. 2-1: Cont.

	BUL1-474-AD **input** (chemical analysis) [mg/l]	**ACW-1** **output (#1)** [mol/kgw]	**ACW-3** **output (#2)** [mol/kgw]
SI(calcite)		-0.16	0
SI(dolomite)		-0.51	-0.17
SI(gypsum)		0.04	0
SI(celestite)		0.21	0
SI(quartz)		0.04	
SI(anhydrite)		-0.17	-0.21

After eliminating the charge misbalance by adjusting the Na^+ concentration, recalculating from 23 °C to 25 °C and imposing saturation equilibrium with celestine, gypsum and calcite, the adjusted solution ACW-3 was obtained by Uni Bern using PhreeqC and Truesdell-Jones activity model and is selected here as input Opalinus Clay water for the calculations described in this report. Note that it is simplified compared to the original analytical solution as bromine, silicon and dissolved organic carbon were excluded in the simplified output #2. In the BPW, however, Si will be reintroduced as it is present in reactive minor minerals in the bentonite inventory (quartz and kaolinite, see Section 2.2.4).

The BPW was modelled using the most advanced version of PSI-Nagra database (Hummel & Thoenen 2022) and the GEM-Selektor code. The latter choice was prompted by the availability of a recently developed model for compacted clay – pore water interaction, dubbed "ClaySor" (Kulik et al., 2018). This model is currently the most advanced tool for modelling clay-water interaction. It implements the 2-Site Protolysis Non-Electrostatic Surface Complexation and Cation Exchange (2SPNE SC/CE) model of Bradbury & Baeyens (2002) and is demonstrably consistent with a large body of in-house sorption data. It will therefore be used to derive sorption coefficients and solubility limits for dose-relevant nuclides in the forthcoming safety assessment calculations. This decision obviously implies, first of all, recalculation of the "OPAw UniBe" water ACW-3 with GEM-Selektor.

In order also to test the robustness of output results, this task was carried out for all six in-built aqueous activity models available in GEM-Selektor and in addition for the SIT activity model described in Section 2.2.2. The results of the recalculations are shown in Tab. 2-2 in comparison with "ACW3 UniBe".

2.2.2 Implementation of Specific Ion interaction Theory (SIT)

Since a detailed description of aqueous activity models is far beyond the scope of the present report, only the salient features and differences will be briefly discussed. A thorough discussion, particularly of the SIT model, can be found in Grenthe et al. (1997). Tab. 2-3 shows the underlying equations of the tested activity models and their range of applicability in terms of ionic strength.

The Davies model is the simplest, as calculation of activity coefficients depends only on temperature (coefficient Aj = 0.51 at 25 °C) ionic strength I and ionic charge z_i. Its application is however limited to dilute solutions (I < 0.01 m). The extended Debye-Hückel equation is the most used activity model in geochemical codes. It has been implemented in different ways, including four of the six variants mentioned in Tab. 2-2 (Truesdell-Jones, Helgeson, Shvarov, Karpov). They differ in the treatment of the parameters $\dot{a}$ (Kielland's ion-size parameter) and b_γ (semi-empirical parameter specific to a given background electrolyte). The other two Debye-Hückel variants (*limiting law* and *no b_gamma*) are simplifications working only for very dilute solutions.

Tab. 2-2: Recalculations of ACW-3 Opalinus Clay pore water from Uni Bern (column 1) using GEM-Selektor and PSI-Nagra thermodynamic database (v. 1207) applying seven different aqueous activity models

The last column (SIT, shaded in yellow) is the variant that will be used for the BPW calculations. Numbers are printed in red whenever the quantity differs by more than 0.05 (pH, I, log pCO_2), 0.1 (SI) or 5% (concentrations) from the original calculation.

	UniBe (PHREEQC)	**LES (GEMS)**	**LES (GEMS)**	**LES (GEMS)**	**LES (GEMS)**	**LES (GEMS)**	**LES (GEMS)**	**LES (GEMS)**
Identifiers								
Calc. ID	ACW3	ACW3a	ACW3a	ACW3a	ACW3a	ACW3a	ACW3a	ACW3a:2
Activity model	DH-Truesdell-Jones	DH-Helgeson	Davies	DH-Shvarov	DH- no b_gamma	DH – limiting law	DH-Karpov	SIT
GEMS project I		BPW-SGT3-1	BPW-SGT3-2	BPW-SGT3-3	BPW-SGT3-5	BPW-SGT3-6	BPW-SGT3	BPW_SIT
pH, ionic strength, temperature, CO_2 partial pressure								
pH	7.27	7.34	7.26	7.37	7.33	8.20	7.29	7.29
T [°C]	25	25	25	25	25	25	25	25
I [eq/kgw]	0.506	0.533	0.489	0.544	0.512	0.594	0.505	0.510
log $p(CO_2)$ [bar]	-2.84	-2.86	-2.78	-2.92	-2.86	-3.85	-2.80	-2.83
Total dissolved elements								
Na	3.46E-01	3.46E-01	3.46E-01	3.46E-01	3.46E-01	3.46E-01	3.46E-01	3.46E-01
K	1.93E-03	1.93E-03	1.93E-03	1.93E-03	1.93E-03	1.93E-03	1.93E-03	1.93E-03
Ca	3.88E-02	4.66E-02	3.58E-02	4.91E-02	4.18E-02	5.09E-02	4.00E-02	3.95E-02
Mg	1.78E-02	1.78E-02	1.78E-02	1.78E-02	1.78E-02	1.78E-02	1.78E-02	1.78E-02
Sr	3.37E-04	4.01E-04	3.08E-04	4.23E-04	3.30E-04	1.53E-03	3.13E-4	3.13E-04
Cl	4.06E-01	4.06E-01	4.06E-01	4.06E-01	4.06E-01	4.06E-01	4.06E-01	4.06E-01
SO_4(tot)	2.77E-02	3.55E-02	2.46E-02	3.80E-02	3.40E-02	4.08E-02	2.88E-2	2.84E-02
CO_3(tot)	8.02E-04	8.47E-04	8.37E-04	8.53E-04	8.46E-04	9.96E-04	8.42E-4	8.42E-4
a(H_2O)	0.986	0.985	0.985	0.985	0.985	0.984	0.985	0.985
Saturation indices of pure solids								
SI(calcite)	0	0	0	0	0	0	0	-0.03
SI(dolomite)	-0.17	-0.85	-0.18	-0.31	-0.21	-0.33	-0.19	-0.26
SI(gypsum)	0	0	0	0	0	0	0	-0.06
SI(celestite)	0	0	0	0	0	0	0	-0.11
SI(anhydrite)	-0.21	-0.21	-0.21	-0.21	-0.21	-1.51	-0.21	-0.27

The SIT formalism is characterized by a summation term describing short-range ion-specific reciprocal interactions. It thus requires in principle interaction coefficients $\varepsilon(i,k)$ between all pairs *i,k* of dissolved species (including uncharged species) in the solution of interest. This requirement is simplified in solutions with a dominating dissolved salt (background electrolyte, e.g. NaCl or $NaClO_4$) as the mutual contributions of minor species is negligible and only interactions with the main cation/anion are needed. In addition, a simplified SIT model assumes that interaction coefficients between equally charged ions are zero and that they are symmetrical, i.e. $\varepsilon(i,k) = \varepsilon(k,i)$. Many such coefficients have been derived from experimental determinations of conditional constants at different ionic strengths e.g. for NaCl, the dominant electrolyte in environmental systems (including Opalinus Clay).

Tab. 2-3: Equations describing the various activity models tested on OPAw

Activity model	**Equation: $\log_{10}\gamma_i =$**	**Ionic strength range**
Davies	$-A_j\, z_i^2 \left(\frac{\sqrt{I}}{1+\sqrt{I}} - 0.3\, I\right)$	0 – 0.1 m
Extended Debye-Hückel	$-\frac{A_j z_i^2 \sqrt{I}}{1 + \dot{a} B_\gamma \sqrt{I}} + b_\gamma I$	0 – 1 m
SIT	$-\frac{A_j z_i^2 \sqrt{I}}{1 + 1.5\sqrt{I}} + \sum_k \varepsilon(i,k)\, m_k$	0 – 6 m

The SIT activity model was preferred and selected here for several reasons. First, it is the method used to extrapolate thermodynamic constants to zero ionic strength for the PSI-Nagra thermodynamic database. Moreover, it is used and recommended by the NEA-TDB project, as summarized in the following citation (Grenthe et al. 2013):

"*This method has been chosen because of its robustness in analysing experimental data from diverse sources, its capacity to provide good estimates of activity coefficients, its simplicity of use and the possibility, by using charge/ion size correlations, to estimate unknown values for its parameters, the so-called ion interaction coefficients*".

Recently, compilations of SIT coefficients, including estimation procedures for unknown coefficients, have been elaborated at LES for the sake of consistent use in geochemical models (Hummel & Thoenen 2022). The interaction coefficients and estimation guidelines described in the aforementioned reports were adopted for the present BPW calculations, resulting in the list of ε-values reported in Appendix 1.

Important advantage of the SIT model are the wide range of ionic strength it covers and the capability of estimating fairly well unknown interaction coefficients from charge/size relationships and other types of correlations (Grenthe et al. 1997). There are of course some limitations, e.g. the necessity of collecting and implementing a large number of interaction parameters in geochemical codes. Moreover, many natural waters cannot be regarded as consisting of a single background electrolyte (e.g. seawater). For the system under consideration here this approximation can be made since NaCl concentrations dominate over all other electrolytes (e.g. KCl, $MgCl_2$, $CaCl_2$, Na_2SO_4).

2.2.3 Definition and selection of selectivity coefficients for cation exchange

Cation exchange is a fundamental process during the equilibration of aqueous solutions with swelling clays such as montmorillonite. Such reactions are triggered by the mild negative structural charge of smectite clay minerals, which requires compensating cations in the expandable interlayer. Ion exchange reactions are fast, reversible and may affect significantly the aqueous composition. Equilibrium is described by law-of-mass-action constants, termed *selectivity coefficients*, applied to reactions such as:

$$2\ NaY + Ca^{2+} \rightleftarrows CaY_2 + 2\ Na^+$$

where "Y" represents an elementary, permanent negative charge in the interlayer of the clay mineral. It may be regarded as a binding site for the exchanged cation.

In spite of decades of studies on cation exchange, there is still no consensus on a unique and thermodynamically sound definition of selectivity coefficients. Several formalisms exist, and great care must be taken to implement a given type of selectivity coefficient correctly in a given code. The most common definitions lead to Gaines-Thomas (K_G) and Vanselow (K_V) selectivity coefficients, defined as follows:

$$K_G \equiv \frac{E_{Ca} a_{Na}^2}{E_{Na}^2 a_{Ca}} \quad (1)$$

$$K_V \equiv \frac{X_{Ca} a_{Na}^2}{X_{Na}^2 a_{Ca}} \quad (2)$$

where a_i, E_i and X_i denote the aqueous activity, equivalent fraction and mole fraction on the clay of cation i, respectively. In previous studies (Curti 1993, Bradbury & Baeyens 2002, Curti & Wersin 2002, Bradbury et al. 2014) Gaines-Thomas selectivity coefficients were applied, since this is the formalism mostly used to interpret experimental cation exchange data. In the light of the discussion in Sections 2.2.1 and 4.3.2 of Kulik et al. (2018), it appears however that Gaines-Thomas coefficients are not true thermodynamic constants, since their values depend on the cation exchange capacity (CEC) and S/W ratio of the system. This shortcoming imposes in geochemical codes the use of operational exchange constants that have to be adjusted whenever CEC and/or or S/W change (see e.g. Eq. 2-11 in Kulik et al. 2018). The Vanselow formulation appears to provide a thermodynamically more sound representation of exchange reactions and was therefore preferred for the "ClaySor" model implemented in GEM-Selektor, which is used and adapted here for the BPW model. Nonetheless, because primary cation exchange data are provided as Gaines-Thomas coefficients, a conversion is necessary to obtain Vanselow coefficients. A generalized conversion equation and its demonstration are provided in Appendix 2 of this report. Tab. 2-4 lists the original Gaines-Thomas coefficients and the converted Vanselow constants used in the present BPW model.

Tab. 2-4: Primary Gaines-Thomas (K_G) and converted Vanselow (K_V) selectivity coefficients for aqueous solution-MX80 bentonite exchange used in the BPW model

K_G values for the Na-Mg, Na-K and Na-Ca exchange reactions were taken from Bradbury and Bayens (2002). K_G values for the Na-Sr and Ba-Sr exchange reactions were set equal to K_G(Na-Ca) based on experimental evidence.

GEM-Selektor species name	Exchange reaction	K_G	K_V
ClayMg@	$2\ NaZ + Mg^{2+} = MgZ_2 + 2\ Na^+$	2.2	1.07
ClayK@	$NaZ + K^+ = KZ + 2\ K^+$	4.0	4.0
ClayCa@	$2\ NaZ + Ca^{2+} = CaZ_2 + 2\ Na^+$	2.6	1.25
ClaySr@	$2\ NaZ + Sr^{2+} = SrZ_2 + 2\ Na^+$	2.6	1.30
ClayBa@	$2\ NaZ + Ba^{2+} = BaZ_2 + 2\ Na^+$	2.6	1.30

2.2.4 Initial state of bentonite

Composition and characteristics of bentonite pore waters will also depend on the "initial state" of the compacted bentonite used as buffer material to seal the repository tunnels. This includes: exchanged cation populations and protonation state of edge sites in montmorillonite at the time of emplacement, as well as the content of reactive minor minerals in bentonite. Knowledge of the "initial state" is particularly important for compacted clay systems (high S/W ratio), as an even small mass transfer from the large amount of solids can have a strong impact on the aqueous phase. In compacted systems, even minor solids may buffer the pore water composition.

To date, no final decision on which bentonite material will be used as repository backfill has been taken. Consequently, as in previous safety assessments, the MX-80 bentonite thoroughly characterized (Müller-Vonmoos & Kahr 1983, Bradbury & Baeyens 2002) is selected here as reference material. Its properties are summarized in Tab. 2-5 and will be used to determine an "initial state" of bentonite for the BPW model calculations presented in this report.

It is important to note that the data in Tab. 2-5 were obtained from few samples of MX-80 bentonite, which may not be representative of natural variations in mineralogy, exchanged cation population and cation exchange capacities. The present BPW model can easily take into account such variations, so that BPW calculations may be easily repeated in future to adapt the results to any type of bentonite material. Moreover, sensitivity analyses may be carried out to assess the influence of mineralogical composition, exchanged cation population and protonation state on the composition and characteristics of equilibrated BPW. These are however not part of the present study.

Tab. 2-5: Initial state of MX-80 bentonite used as reactant material in the calculation of BPW composition

GEMS name	Species/mineral	mol/kg	Site fraction*	Mole fraction
Amphoteric edge sites				
= SsO-	$= S^{S}O^{-}$	8.5×10^{-4}	0.567	0.567
= SsOH@	$= S^{S}OH$	6.5×10^{-4}	0.433	0.433
= SsOH2+	$= S^{S}OH_2^{+}$	2.1×10^{-7}	1.4×10^{-4}	1.4×10^{-4}
Ess	$= S^{S}$(total)	1.5×10^{-3}	1	1
= SvO-	$= S^{W1}O^{-}$	1.7×10^{-2}	0.567	0.567
= SvOH@	$= S^{W1}OH$	1.3×10^{-2}	0.433	0.433
= SvOH2+	$= S^{W1}OH_2^{+}$	4.2×10^{-6}	1.4×10^{-4}	1.4×10^{-4}
Esv	$= S^{W1}$(total)	3.0×10^{-2}	1	1
= SwO-	$= S^{W2}O^{-}$	3.0×10^{-4}	0.010	0.010
= SwOH@	$= S^{W2}OH$	2.96×10^{-2}	0.987	0.987
= SwOH2+	$= S^{W2}OH_2^{+}$	9.4×10^{-5}	0.003	0.003
Esw	$= S^{W2}$(total)	3.0×10^{-2}	1	1
Exchanged ions				
NaClay@	NaZ	0.668	0.843	0.907
KClay@	KZ	0.013	0.016	0.018
MgClay@	MgZ_2	0.020	0.051	0.027
CaClay@	CaZ_2	0.033	0.083	0.045
SrClay@	SrZ_2	0.002	0.005	0.003
BaClay@	BaZ_2	5×10^{-4}	0.001	0.001
Clay-	Z(total)	CEC = 0.792[&]	1	1
Reactive minor minerals[+]				
gypsum		0.0235		
quartz		1.66		
kaolinite		0.039		
calcite		0.3		
siderite		0.086		
magnetite		0.43		

* Same as equivalent fraction for exchanged cations.

& The cation exchange capacity (CEC) is slightly higher than 0.787 eq/kg given by Bradbury & Baeyens (2002) because of the addition of small capacities for Ba^{2+} and Sr^{2+}. This deviation lies within the uncertainty of the CEC determination.

+ Same inventories as assumed in SGT2 BPW project.

2.2.5 Definition of Solid/Water (S/W) ratio based on anion porosity

As previously discussed in Section 2.1, in the model only "interparticle" water is assumed to equilibrate with minor minerals in bentonite. The interlayer water is not in direct contact with minor minerals and thus excluded from the equilibrium calculations. Montmorillonite is treated as a pure cation exchanger with amphoteric edge sites and is considered to be insoluble. This approximation is based on experimental work indicating that only minor amounts of Al and Si are released in dissolution experiments (May et al. 1986, Kittrick & Peryea 1988, Curti 1993). Moreover, the aqueous concentrations of these elements are limited at low values by kaolinite, gibbsite and SiO_2 equilibria, so that solubility products based on reversible precipitation/ dissolution experiments could not be measured so far.

The interparticle water consists of uncharged water (defined by the "anion accessible" porosity ε_{an}) and a "diffuse double layer" (DDL) of positively charged water, in which excess cations balance the negative surface charge of montmorillonite dominate and most anions are excluded. The DDL has a thickness ranging from hundreds of nanometers to a few micrometers, with thickness depending inversely on the ionic strength. The higher the ionic strength, the thinner the DDL and the larger the proportion of uncharged water defining the anion accessible porosity. At ionic strengths exceeding 1 – 2 m the DDL thickness reaches a minimum, corresponding to a limiting (maximum) value $\varepsilon_{an,max}$, which is equal to the difference between total porosity ε_{tot} and interlayer porosity ε_{IL}.

Based on experimental data with conservative tracers, Van Loon (2012) derived the following empirical equations to determine the aforementioned porosities as a function of ionic strength (I [mol/kgw]) and the degree of clay compaction (expressed by the dry bulk density of the clay, ρ_b [m^3 kg^{-1}]):

$$\varepsilon_{an,max} = 3.964 \times 10^{10}\, {\rho_b}^{-3.6031} \quad (3)$$

$$\varepsilon_{an} = \varepsilon_{an,max} - A \exp(-B\, I) \quad (4)$$

where:

$$A = 2.038 \times 10^{10} + 10\, {\rho_b}^{-3.5328} \quad (5)$$

$$B = -0.24 - 0.00695\rho_b + 3.5 \times 10^{-6}\, {\rho_b}^2 \quad (6)$$

The total porosity, ε_{tot} [-] is defined as the volume occupied by interlayer, anion porosity and DDL divided by the total volume of the clay. It is related to the bulk dry density (ρ_b) and mineral grain density (ρ_g) by:

$$\varepsilon_{tot} = 1 - \frac{\rho_b}{\rho_g} \quad (7)$$

Based on the above equations, and assuming an ionic strength of 0.61 m the values given in Tab. 2-6 were determined for dry bulk densities of 1'450, 1'300, 1'600 kg m^{-3}. The latter two values were used in SGT-2 BPW calculations, whereas 1'450 kg m^{-3} is the current provisional value supplied by Nagra for SGT-3 BPW calculations. The ionic strength of 0.61 m was selected as typical value obtained for the BPWs, as shown later. The results in Tab. 2-6 indicate anion

porosities varying between 9% and 21.2% for bentonite compactions between 1'300 and 1'600 kg m^{-3}, implying that only about 20% to 40% of the total water taken up in saturated MX-80 bentonite is charge-neutral interparticle water[3]. This figure increases to 26% to 45% if also DDL water is taken into account.

Tab. 2-6: Total porosity, maximum anion accessible porosity and anion accessible porosity at I = 0.61 m for 3 different degrees of compaction of MX-80 bentonite

Based on VanLoon (2012)

ρ_b (kg m^{-3}) = >	1300	1450	1600
ε_{tot}	0.536	0.482	0.429
$\varepsilon_{an,max}$	0.239	0.161	0.113
ε_{an}	0.212	0.138	0.090

Fig. 2-2 shows the continuous variation of ε_{an} as a function of ionic strength for the 3 dry densities specified in Tab. 2-6 based on the treatment described by Van Loon (2012). The plot shows that at ionic strengths around 0.6 m the DDL thickness is already close to its minimum value, implying that the anion porosity is close to $\varepsilon_{an,max}$. This means that the dominant fraction of interparticle water consists of uncharged free aqueous solution. Any further increase in ionic strength would modify the proportions of uncharged and DDL water only slightly.

Fig. 2-3 shows the calculated volumetric distribution of the various water types and solid in compacted clays for the three aforementioned bulk dry densities. In all cases, the largest part of the volume is occupied by water-saturated clay ("mineral" + "interlayer"). Note that the fractional volume of solid ("mineral") represents only the volume occupied by structural TOT units and exchanged ions, while "interlayer" corresponds to the volume of water residing in the interlayer of the swelled montmorillonite. The interparticle water consists, depending on the compaction, of 9% – 21% of anion accessible water and only 2% – 3% DDL water with an excess positive charge balancing the negative clay surface charge.

In the "ClaySor" model (Kulik et al. 2018) the DDL is taken into account implicitly by including the associated cation or anion excess in the calculated bulk pore water composition. In highly compacted systems, this approach leads, depending on pH, to solutions with a more or less significant excess of positive or negative charge in the aqueous phase. Therefore, for the present BPW calculations the (S/W) ratio will be determined based on the maximum anion accessible porosity $\varepsilon_{an,max}$, i.e. including the DDL volume in the aqueous phase. This leads in the systems of interest to slightly lower S/W ratios compared to calculations in which the reactive water volume is defined by ε_{an} , as evident from Fig. 2-3.

[3] These values are obtained by dividing anion porosity by total porosity.

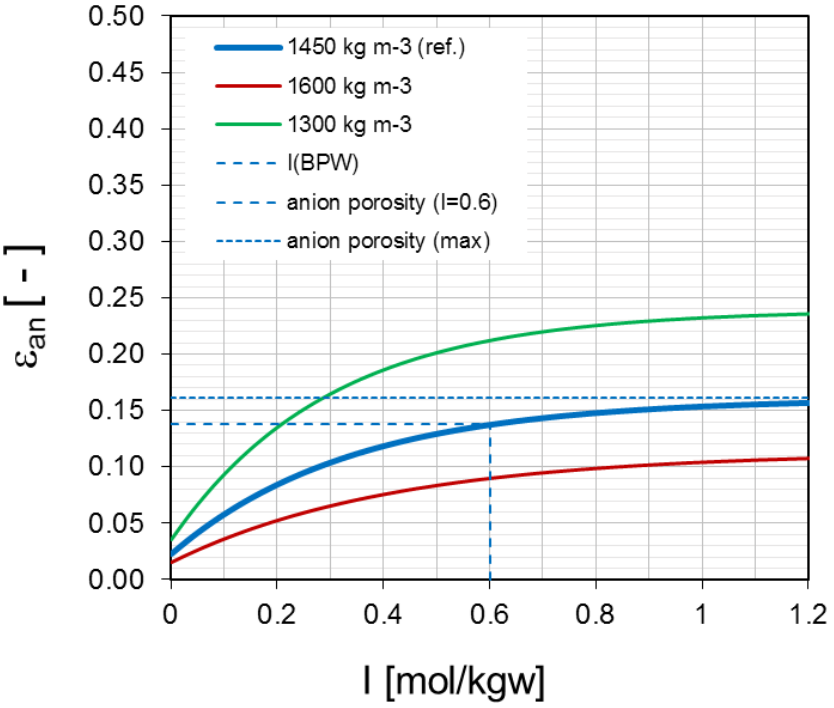

Fig. 2-2: Anion accessible porosities as function of ionic strength for MX-80 bentonite with 3 different degrees of compaction. The vertical broken line marks the approximate ionic strength of calculated BPW (I = 0.6 m, see later)

Horizontal broken lines mark the values of anion accessible porosity at I = 0.6 m for a clay dry density of 1'450 kg/m^3 and the corresponding limiting value at high ionic strength ($\varepsilon_{an,max}$).

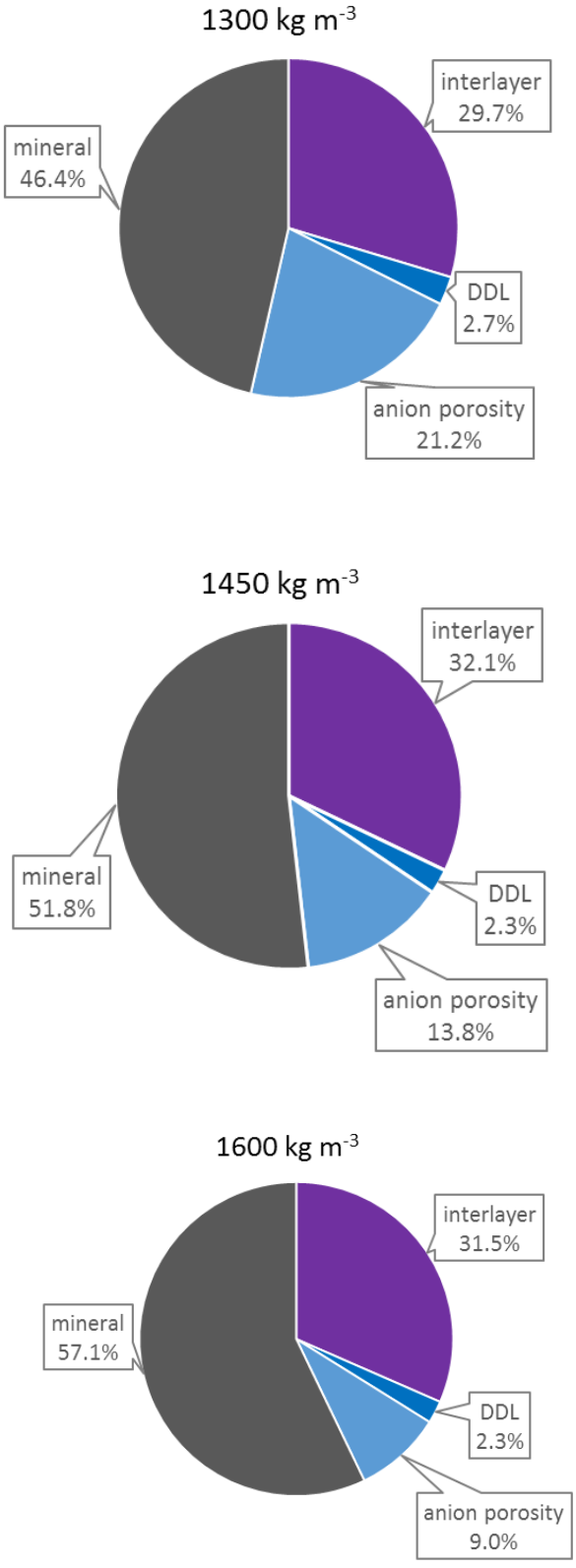

Fig. 2-3: Volumetric distribution of water types and solid in compacted bentonite for three different dry bulk densities

2.3 Model implementation in GEM-Selektor

2.3.1 Definition of GEM-Selektor input

The "ClaySor" model adapted for the BPW calculations has been implemented into the GEM-Selektor code (v. 3.7.0) (Kulik et al. 2013). In this Section, we document technical practicalities of the implementation, starting from the construction of an input file.

The first step is to define the reacting entities, such as the input aqueous solution (Opalinus Clay porewater, shortly OPAw) and the MX-80 bentonite in its initial state. To this aim, GEM-Selektor offers the so-called COMPOS utility, which allows defining "en bloc" all necessary constituents of a given phase as a single input entity scaled to a pre-defined amount. They may be entered in the desired amounts in the "input recipe" window, eliminating the tedious task of specifying for each calculation all single constituents of the COMPOS.

Fig. 2-4 shows the COMPOS defining the selected OPAw (ACW3a) scaled to 1 kg of water solvent (1.02719 kg of solution). The solution is defined in terms of moles of the listed elements, taken from the output of the ACW3a calculation.

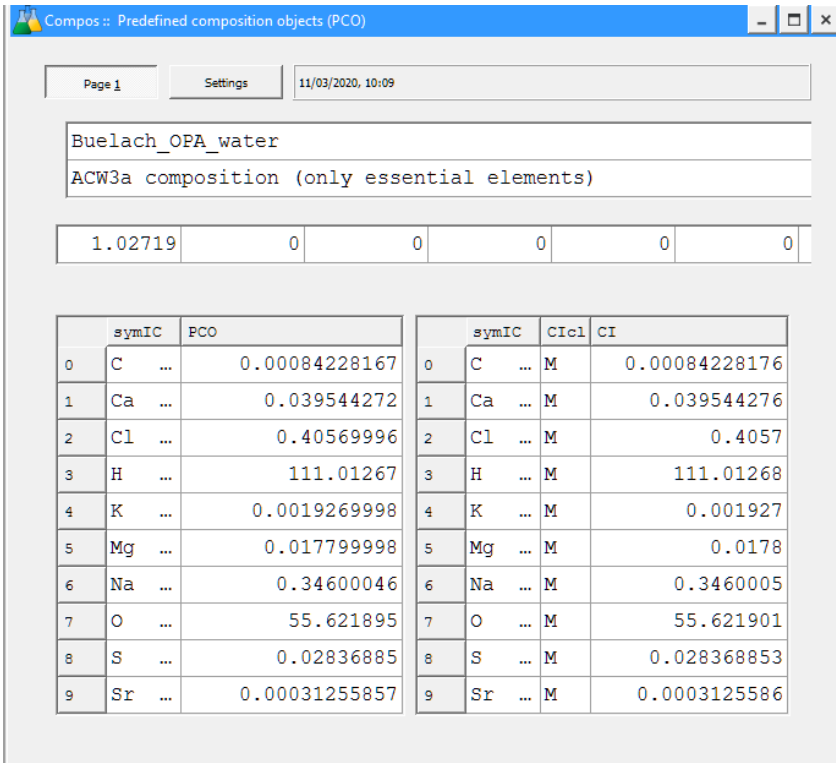

	symIC	PCO
0	C ...	0.00084228167
1	Ca ...	0.039544272
2	Cl ...	0.40569996
3	H ...	111.01267
4	K ...	0.0019269998
5	Mg ...	0.017799998
6	Na ...	0.34600046
7	O ...	55.621895
8	S ...	0.02836885
9	Sr ...	0.00031255857

	symIC	CIcl	CI
0	C ...	M	0.00084228176
1	Ca ...	M	0.039544276
2	Cl ...	M	0.4057
3	H ...	M	111.01268
4	K ...	M	0.001927
5	Mg ...	M	0.0178
6	Na ...	M	0.3460005
7	O ...	M	55.621901
8	S ...	M	0.028368853
9	Sr ...	M	0.0003125586

Fig. 2-4: COMPOS entry for provisional Bülach water ACW3a, used as reacting water in the BPW calculations

The second step consisted in defining the initial populations of exchanged cations in montmorillonite for exactly 1 kg of MX-80 bentonite. Fig. 2-5a shows the corresponding "MX80_exch" COMPOS, defined in terms of the elements forming exchangeable dissolved cations (Ba, Ca, K, Mg, Na, Sr) and the independent component (IC) [4] "Clay", which quantifies exchangeable sorption sites according to the data given in Bradbury & Baeyens (2002), Tab. A8. "MX80_full" (Fig. 2-5b) is an analogous COMPOS entry, including in addition to exchangeable elements the scaled amounts of amphoteric surface sites (= S^s, = S^{W1} and = S^{W2}) as ICs Ess, Esv and Esw, respectively. Because ICs are by definition charge-neutral, such an input is equivalent to specifying an initial state in which the three amphoteric sites are fully occupied by neutral species, i.e. 100% = S^sOH, = $S^{W1}OH$, = $S^{W2}OH$, whereas deprotonated species (= S^sO^-, = $S^{W1}O^-$, = $S^{W2}O^-$) and doubly protonated species (= $S^sOH_2^+$, = $S^{W1}OH_2^+$, = $S^{W2}OH_2^+$) are absent. Such initial distribution is however unrealistic and does not correspond to the initial surface site speciation in Tab. 2-5.

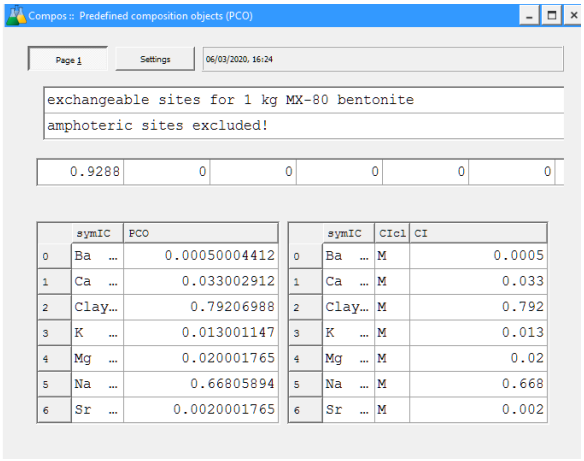
Compos :: Predefined composition objects (PCO)

Page 1 | Settings | 06/03/2020, 16:24

exchangeable sites for 1 kg MX-80 bentonite
amphoteric sites excluded!

0.9288	0	0	0	0	0

	symIC	PCO
0	Ba …	0.00050004412
1	Ca …	0.033002912
2	Clay…	0.79206988
3	K …	0.013001147
4	Mg …	0.020001765
5	Na …	0.66805894
6	Sr …	0.0020001765

	symIC	CIcl	CI
0	Ba …	M	0.0005
1	Ca …	M	0.033
2	Clay…	M	0.792
3	K …	M	0.013
4	Mg …	M	0.02
5	Na …	M	0.668
6	Sr …	M	0.002

a (MX80_exch)

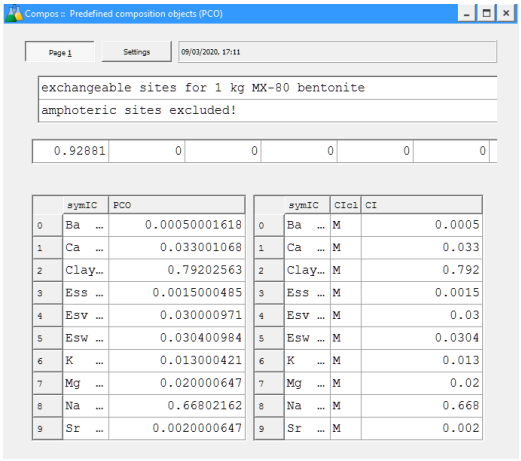
Compos :: Predefined composition objects (PCO)

Page 1 | Settings | 09/03/2020, 17:11

exchangeable sites for 1 kg MX-80 bentonite
amphoteric sites excluded!

0.92881	0	0	0	0	0

	symIC	PCO
0	Ba …	0.00050001618
1	Ca …	0.033001068
2	Clay…	0.79202563
3	Ess …	0.0015000485
4	Esv …	0.030000971
5	Esw …	0.030400984
6	K …	0.013000421
7	Mg …	0.020000647
8	Na …	0.66802162
9	Sr …	0.0020000647

	symIC	CIcl	CI
0	Ba …	M	0.0005
1	Ca …	M	0.033
2	Clay…	M	0.792
3	Ess …	M	0.0015
4	Esv …	M	0.03
5	Esw …	M	0.0304
6	K …	M	0.013
7	Mg …	M	0.02
8	Na …	M	0.668
9	Sr …	M	0.002

b (MX80_full)

Fig. 2-5: GEM-Selektor input specification of montmorillonite for 1 kg of MX-80 bentonite
(a) only exchanged cations, (b) exchanged cations with amphoteric sites

In order to comply with the data in Tab. 2-5, the simpler "MX80_exch" COMPOS was used in combination with an explicit specification of species distribution on the amphoteric sites. This was achieved by introducing in the recipe window (Fig. 2-6) the experimentally determined amounts of the nine =SOH-type adsorbed species listed in Tab. 2-5. Note that only protonation/deprotonation adsorption reactions are considered explicitly in the BPW model. Metal complexation reactions are neglected, but these may be easily added when necessary (and provided that data are available) in future calculations of radionuclide sorption Kd's.

[4] In the technical language of GEMS, an independent component (IC) is the basic entity from which by combination with other ICs species are constructed. ICs are typically chemical elements, but can also define the substrates for specific surface sites or ion exchange sites.

The explicit specification of = SOH site occupancies forcefully leads to a net negative charge of the overall system to be equilibrated. In the case illustrated in Fig. 2-6, a net surface charge of -18.0516 millimoles, representing the non-permanent (pH-dependent) surface charge of the clay, is generated in the input system. This negative charge is balanced by adding a corresponding amount of sodium ions (entry "Na+" in Fig. 6), which represents the excess of positive ions in the DDL.

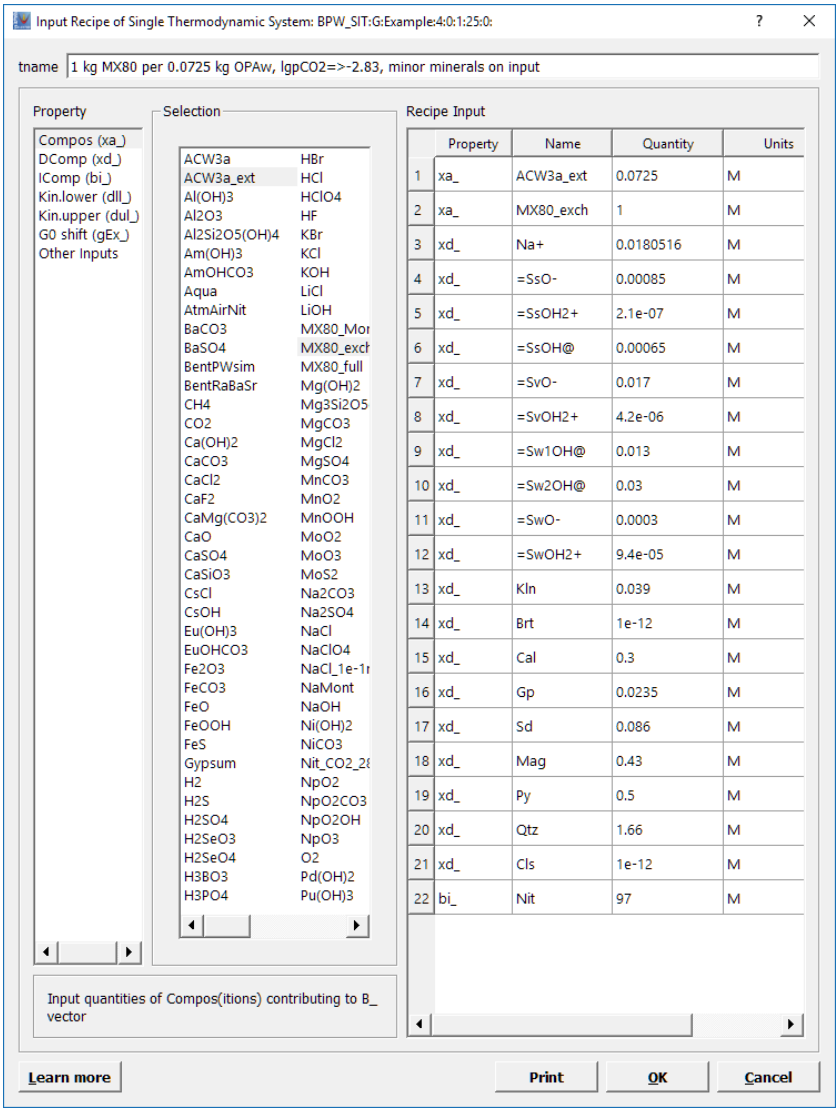

Fig. 2-6: Typical recipe input window for BPW model calculations. The specified units (M) are moles for all species except the COMPOS ACW3_ext and MX80_exch, for which 1 M corresponds exactly to 1 kg of aqueous solution and 1 kg of dry MX-80 bentonite, respectively

The "input recipe" window also includes specific amounts of minor minerals (Kln = kaolinite, Brt = baryte, Cal = calcite, Gp = gypsum, Sd = siderite, Mag = magnetite, Py = pyrite, Qtz = quartz, Cls = celestine) which are required to react with MX-80 bentonite and OPAw. These minerals were all detected in MX-80 except for magnetite, which represents canister corrosion products. The specified amounts were derived from the MX-80 characterization data of Müller-Vonmoos & Kahr (1983) and Bradbury & Baeyens (2002) and correspond to those assumed in the SGT-2 BPW calculations (Bradbury et al. 2014).

In order to define the desired degree of compaction in the "recipe window", the corresponding maximum anion porosity for the system of interest must be converted to a mass of OPAw solution. For instance, to represent $\varepsilon_{an,max}$ = 0.113 for a bulk dry density of ρ_b = 1'600 kg m^{-3}, the following conversion formula can be used:

$$m_{aq} = \frac{\rho_{aq}\, \varepsilon_{an,max}\, m_{clay}}{\rho_b} \tag{8}$$

where m_{aq} is the mass of aqueous solution (the entire solution, not just the solvent), m_{clay} the mass of dry clay and ρ_{aq} = 1'026 kg m^{-3} the density of the BPW[5]. Because the mass of dry clay in the GEM-Selektor recipe window is fixed to 1 kg[6], the formula simplifies further and one obtains, for a dry bulk density of 1'600 kg m^{-3}:

$$m_{aq} = \frac{\rho_{aq}\, \varepsilon_{an,max}}{\rho_b} \times 1\ kg = \frac{1026 \times 0.113}{1600} = 0.0725\ kg = 72.5\ g \tag{9}$$

From this, the following *S/W* ratio [kg/l] is readily derived:

$$S/W = \frac{\rho_{aq}\, m_{clay}}{m_{aq}} = \frac{1.026\ kg/l \times 1000\ g}{72.5\ g} = 14.15\ kg/l \tag{10}$$

Tab. 2-7 lists the input values of m_{aq} in GEM-Selektor's recipe window for the three considered degrees of compaction considered so far and the corresponding *S/W* ratios.

The last entry in the recipe window shown in Fig. 2-6 ("Nit" = 97 M) requires equilibration with 97 moles of non-reactive nitrogen. This is a simple method to constrain the aqueous solution to be in equilibrium with a pre-defined CO_2 partial pressure. In the illustrated example, the amount of non-reactive N_2 ("Nit") was increased by trial and error until the initially high pCO_2 decreased to the target value of $10^{-2.83}$ bar. This value was reached at the addition of 97 mol of "Nit". The CO_2 is generated by outgassing following calcite dissolution during the overall equilibration process.

---

[5] This is the density of aqueous solution calculated from GEM-Selektor for a typical BPW water with 0.6 m ionic strength.

[6] Fixing the amount of clay is practical, as it avoids rescaling the = SOH sites at each new calculation. Only the amount of water must be changed.

Tab. 2-7: Determination of OPAw input amounts and corresponding S/W ratios from eqs. (9) and (10) for three different degrees of compaction

Input eqs. (9), (10)				
ρ_b	1'300	1'450	1'600	[kg m^{-3}]
$\varepsilon_{an,max}$	0.239	0.161	0.113	[-]
ρ_{aq}	1'026	1'026	1'026	[kg m^{-3}]
Results eqs. (9), (10)				
m_{aq} (input ACW3a_ext)	0.1886	0.1141	0.0725	[kg]
S/W	5.44	9.00	14.15	[kg l^{-1}]

2.3.2 Brief description of GEM-Selektor output

Fig. 2-7 shows an example of GEM-Selektor output from the BPW calculation with the input defined in Fig. 2-6. After checking the input for charge balance with the dedicated button (green circle), the calculation is started by clicking on the "Calculate" button (encircled in red). By default, the window with yellow border pops up with some essential results (number of iterations, masses of gas, aqueous and solid phases, pH, pe and ionic strength). After clicking on accept, the detailed results can be examined by inspecting the "EqStat" and "EqDemo" windows. Part of the output file is shown in Fig. 2-8.

Output files are generated using in-built print scripts that can be activated from the "Print" command of GEM-Selektor menu at the top left of the program window. Fig. 2-8, Page 1, shows the input composition (B-vector), mass balance accuracy and the calculated chemical potentials. On Page 2, the dissolved elemental concentrations at equilibrium are listed in different units. Finally, Page 3 and Page 4 report the equilibrium concentrations, activities and activity coefficients of all gaseous and dissolved species, exchanged cations, surface hydroxyl species and solid phases.

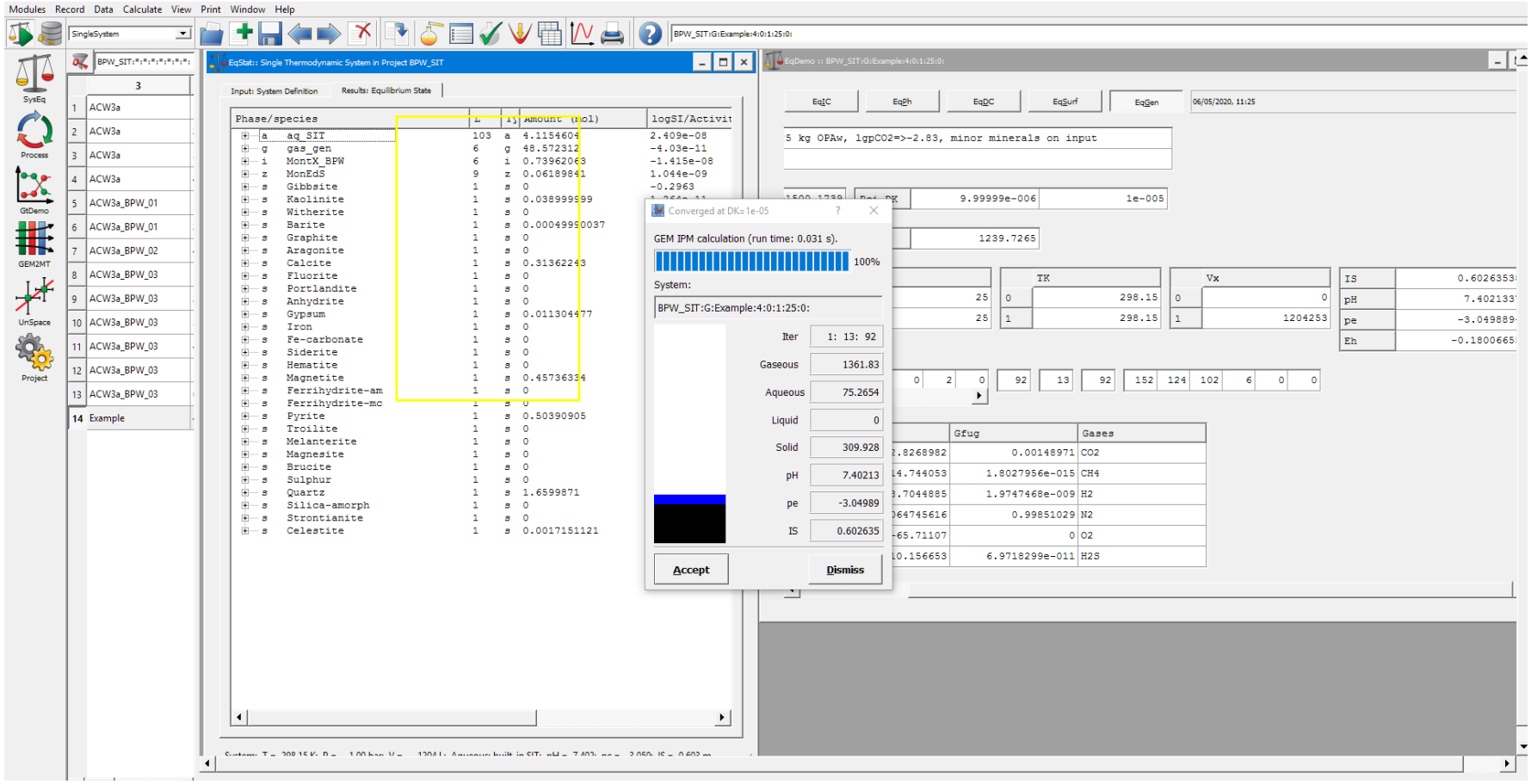

Fig. 2-7: GEM-Selektor screenshot after successful BPW calculation

GEM-Selektor v.2-PSI: Calculation of Equilibrium State in the System:
BPW_SIT:G:Example:4:0:1:25:0: 06/05/2020 16:14

1 kg MX80 per 0.0725 kg OPAw, lgpCO2=>-2.83, minor minerals on input
`
State variables: P(bar)= 1 T= 25 (C) = 298.15 (K) V(cm3)= 1204253
Mass(kg)= 2.676824886 Min.potential (moles): G(x)= -1500.17389

Table 1
Parameters of Independent Components (IC, Stoichiometry Units)

IC Name	Input bulk composition, moles (b)	Deviation of mass balance (Cb)	IC chemical potential mol/mol (u)	IC chemical potential J/mol (ue)
Al	0.07800000007	0	-207.9599	-515526.5
Ba	0.0005000441907	0	-229.9131	-569947.9
Br	7.249999258e-011	0	-70.13059	-173851.7
C	0.3860610648	0	-14.29928	-35447.5
Ca	0.3593698694	-2.736e-017	-214.2446	-531106.2
Cl	0.02941325699	0	-61.21286	-151744.9
Clay	0.7920698816	9.608e-017	-2.029902	-5032.1
Ess	0.00150021	0	-14.00067	-34707.3
Esv	0.0300042	3.42e-018	-11.00494	-27280.9
Esw	0.030394	-8.55e-019	-10.75479	-26660.8
F	7.249999258e-011	-3.605e-027	-142.1382	-352356.5
Fe	1.876	-1.094e-016	-35.93546	-89083.0
H	8.342265433	4.925e-016	-10.02141	-24842.8
K	0.01314085453	0	-113.3265	-280933.1
Mg	0.02129226456	0	-174.7281	-433145.8
Na	0.7111955743	1.094e-016	-99.68589	-247118.4
Nit	97	0	-0.0007454115	-1.8
O	10.78448583	-1.154e-015	-75.65267	-187540.8
S	1.02555674	2.586e-016	-16.95906	-42041.0
Si	1.738	0	-193.5123	-479711.4
Sr	0.002022836937	-2.138e-019	-223.458	-553945.9
Zz	0	2.138e-018	-7.02263	-17408.9

Aqueous phase: I(molal)= 0.6026 pH= 7.402 pe= -3.05 Eh(V)= -0.1801

Table 1A
Total Dissolved Independent Components

IC Name	Molality (mol/kgH2O) (m_t)	log m molality (lgm_t)	log M molarity (recalc.)	Concentration (g/kg-soln) (w_t)
Al	1.646199e-008	-7.78352	-7.78757	4.298058e-007
Ba	1.510735e-007	-6.82081	-6.82487	2.007569e-005
Br	9.954504e-010	-9.00198	-9.00604	7.69682e-008
C	0.00109806	-2.95937	-2.96343	0.01276208
Ca	0.02874623	-1.54142	-1.54548	1.114834
Cl	0.4038544	-0.393775	-0.397832	13.85482
Clay	0	0	0	0
Ess	0	0	0	0
Esv	0	0	0	0
Esw	0	0	0	0
F	9.954504e-010	-9.00198	-9.00604	1.830037e-008
Fe	1.292573e-005	-4.88854	-4.8926	0.0006984937
H	0.001032205	-2.98623	-2.99029	0.001006765
K	0.002576537	-2.58896	-2.59302	0.09748042
Mg	0.02034881	-1.69146	-1.69552	0.4785836
Na	0.5077127	-0.294382	-0.298439	11.29474
Nit	0.001274315	-2.89472	-2.89878	0.01727173
O	0.2353236	-0.628335	-0.632392	3.643279
S	0.05793044	-1.23709	-1.24115	1.797581
Si	0.0001776381	-3.75046	-3.75452	0.004827713
Sr	0.000249614	-3.60273	-3.60679	0.02116388
Zz	0.08822079	-1.05443	-1.05849	0

Fig. 2-8: Screenshot of GEM-Selektor BPW output file (example calculation)

Parameters of Dependent Components (DC, Species)

Species name	type	Quantity in the system	Concentration	Activity coeff.	log activity	Chemical potential
DCnam	DCC	x (moles)	my or Wxx	gamma	lga	fx(J/mol)
Al(SO4)+	S	8.49613e-015	1.1665e-013	0.699	-13.09	-535
Al(SO4)2-	S	5.12007e-015	7.03e-014	0.6304	-13.35	-840
Al+3	S	4.44712e-015	6.106e-014	0.03092	-14.72	-229
AlF+2	S	3.66404e-018	5.0309e-017	0.2161	-16.96	-364
AlF2+	S	2.4235e-022	3.3275e-021	0.699	-20.63	-499
AlF3@	S	8.94397e-028	1.228e-026	1.018	-25.9	-634
AlF4-	S	2.23848e-034	3.0735e-033	0.6304	-32.71	-769
AlF5-2	S	0	0	0.1678	-41.02	-905
AlF6-3	S	0	0	0.01919	-50.34	-1040
AlO+	S	3.13719e-012	4.3075e-011	0.699	-10.52	-291
AlO2-	S	1.11809e-009	1.5352e-008	0.6369	-8.01	-352
AlO2H@	S	7.75231e-011	1.0644e-009	1.018	-8.965	-369
AlOH+2	S	1.74196e-013	2.3918e-012	0.2161	-12.29	-308
AlHSiO3+2	S	1.10229e-014	1.5135e-013	0.2161	-13.49	-652
AlSiO5-3	S	1.02382e-019	1.4057e-018	0.01919	-19.57	-759
Ba(CO3)@	S	4.82246e-013	6.6214e-012	1.018	-11.17	-471
Ba(HCO3)+	S	1.10077e-011	1.5114e-010	0.699	-9.976	-488
Ba(SO4)@	S	3.83885e-009	5.2709e-008	1.018	-7.27	-549
Ba+2	S	7.15254e-009	9.8207e-008	0.2006	-7.706	-244
BaOH+	S	1.72474e-015	2.3681e-014	0.699	-13.78	-323
Ca(CO3)@	S	3.97102e-007	5.4524e-006	1.018	-5.256	-456
Ca(HCO3)+	S	3.7182e-006	5.1052e-005	0.699	-4.448	-473
Ca(SO4)@	S	0.000388164	0.0053296	1.018	-2.266	-534
Ca+2	S	0.00170134	0.02336	0.2141	-2.301	-228
CaF+	S	2.07501e-012	2.8491e-011	0.7322	-10.68	-363
CaOH+	S	2.14488e-009	2.945e-008	0.699	-7.686	-307
Ca(HSiO3)+	S	5.69563e-009	7.8203e-008	0.699	-7.262	-652
CaSiO3@	S	1.15989e-011	1.5926e-010	1.018	-9.79	-635
Fe(CO3)@	S	2.39863e-009	3.2934e-008	1.018	-7.475	-277
Fe(HCO3)+	S	1.28885e-008	1.7696e-007	0.6672	-6.928	-294
Fe(HSO4)+	S	5.53715e-014	7.6027e-013	0.699	-12.27	-373
Fe(SO4)@	S	1.4596e-007	2.0041e-006	1.018	-5.69	-356
Fe+2	S	6.98231e-007	9.587e-006	0.2201	-5.676	-50
OH-	S	2.58709e-008	3.5522e-007	0.6982	-6.606	-79
H+	T	3.86776e-009	5.3106e-008	0.746	-7.402	-17
H2O@	W	4.04275	0.98233	0.9997	-0.00788	-96
CO2	G	0.0723587	0.0014897	1	-2.827	-166
CH4	G	8.7567e-014	1.8028e-015	1	-14.74	-54
H2	G	9.59183e-008	1.9748e-009	1	-8.704	-20
N2	G	48.5	0.99851	1	-0.0006475	-0
O2	G	0	0	1	-65.71	-151
H2S	G	3.38638e-009	6.9718e-011	1	-10.16	-37
ClayBa@	M	1.32821e-007	1.7958e-007	1	-6.746	-234
ClayCa@	M	0.0323493	0.043738	1	-1.359	-218
ClayK@	M	0.0129532	0.017513	1	-1.757	-115
ClayMg@	M	0.0198102	0.026784	1	-1.572	-179
ClayNa@	M	0.674218	0.91157	1	-0.04021	-102
ClaySr@	M	0.000289545	0.00039148	1	-3.407	-228
=SsO-	U	0.000361382	0.0058383	1	-2.234	-83
=SsOH2+	U	1.42535e-006	2.3027e-005	1	-4.638	-117
=SsOH@	U	0.0011374	0.018375	1	-1.736	-100
=SvO-	U	0.00722765	0.11677	1	-0.9327	-80
=SvOH2+	U	2.84956e-005	0.00046036	1	-3.337	-114
=Sw1OH@	U	0.0227481	0.36751	1	-0.4347	-97
=Sw2OH@	U	0.0292135	0.47196	1	-0.3261	-96
=SwO-	U	2.33236e-005	0.0003768	1	-3.424	-79
=SwOH2+	U	0.00115719	0.018695	1	-1.728	-113
Gbs	O	0	0	1	-0.2963	-465
Kln	O	0.039	1	1	1.264e-011	-1524
witherite	O	0	0	1	-5.323	-471
Brt	O	0.0004999	1	1	1.159e-009	-549
Gr	O	0	0	1	-6.21	-14
Arg	O	0	0	1	-0.1438	-456
Cal	O	0.313622	1	1	1.14e-008	-456
Fl	O	0	0	1	-10.34	-499
Portlandite	O	0	0	1	-10.31	-386
Anh	O	0	0	1	-0.2082	-534
Gp	O	0.0113045	1	1	-2.075e-006	-725
Fe	O	0	0	1	-15.61	-36
FeCO3(pr)	O	0	0	1	-1.405	-277
Sd	O	0	0	1	-0.9646	-277
Hem	O	0	0	1	-0.221	-299
Mag	O	0.457363	1	1	1.308e-010	-410
Fe(OH)3(am)	O	0	0	1	-4.562	-293
Fe(OH)3(mic)	O	0	0	1	-2.562	-293
Py	O	0.503909	1	1	-8.177e-012	-70
Tro	O	0	0	1	-3.728	-53
Melanterite	O	0	0	1	-5.784	-1025
Mgs	O	0	0	1	-0.34	-416
Brc	O	0	0	1	-4.5	-346
Sulfur	O	0	0	1	-7.365	-17
Qtz	O	1.65999	1	1	-1.975e-013	-345
Amor-Sl	O	0	0	1	-1.032	-345
Str	O	0	0	1	-1.276	-465
Cls	O	0.00171511	1	1	1.123e-006	-543

Fig. 2-8: Cont.

3 BPW calculations: model testing (TDB 12/07)

3.1 Database and parameter variations

3.1.1 Database, activity model and treatment of minerals

All calculations discussed in this section of the report were carried out using the former version 12/07 of PSI-Nagra database (Thoenen et al. 2014), implemented in Version 3.7.0 of GEM-Selektor. The updated database TDB 2020 (Hummel & Thoenen 2022) was not yet available at the time when calculations were carried out. Activity coefficients of aqueous species were calculated based on the Specific ion Interaction Theory (SIT), using the interaction coefficients ($\varepsilon_{j,k}$) listed in Appendix 1. The reasons for selecting SIT are discussed in Section 2.2.2.

For these BPW calculations, the following simplifying assumptions have been made concerning the treatment of mineral-aqueous solution equilibria:

a) For consistency reasons and as in previous BPW models, only pure minerals have been considered, i.e. there is no solid solution equilibrium involved. This is because reliable solid solution data are not available for all minerals relevant for the system under consideration (carbonates, sulphates, Fe sulphides and oxides, clay minerals).

b) Two mineral phases have been thus purposely excluded as potentially precipitating phases (i.e. deactivated in GEM-Selektor): dolomite, $CaMg(CO_3)_2$, and goethite, FeOOH. Dolomite formation at low temperature is known to be kinetically inhibited at low temperature and requires special conditions (Arvidson & MacKenzie 1999, Roberts et al. 2013). The reasons for excluding goethite are more subtle and are explained in the special Section devoted to Fe-bearing phases and redox control (Section 3.2.6).

Finally, in the PSI-Nagra database 12/07 (unlike other databases such as Thermoddem, see Blanc et al. 2012) no clay minerals except kaolinite were yet included, although such minerals may slowly react in aqueous solutions at low temperatures. The main reason for this choice was the absence of reliable solubility data proving that complex clay minerals (typically smectites and illites) can be treated as fixed-composition phases that reach a well-defined equilibrium both from supersaturation and undersaturation. Consequently, our model considers montmorillonite as a pure, stable cation exchanger phase that does not undergo significant dissolution/precipitation reactions. This assumption is in agreement with data showing that smectites do not undergo illitisation and remain stable at temperatures below about 100 °C. In TDB 2020, a series of clay mineral data taken from Thermoddem will be included. These (unreviewed) data will however not be included in the definitive BPW model calculations for the aforementioned reasons.

3.1.2 Parameter variations

The main purpose of the present calculations was to test the BPW model, using current available data. Key parameters known to potentially affect pH, ionic strength and composition of the BPW were varied with respect to a single source case[7] calculation that uses a single provisional OPAw composition derived from analyses of water extracts from the Bülach borehole, denoted ACW3a and discussed in Section 2. All calculations were carried out at standard state conditions (25 °C, 1 bar) in order to keep consistency with future calculations of solubility limits and sorption coefficients of dose-relevant radionuclides, for which reliable extrapolations to repository temperatures are currently not possible.

An overview of the performed BPW calculations is provided in Tab. 3-1. Basically, the parameter variations explore the effect of bentonite pre-compaction, of pCO_2 constraints and evolution with increasing amounts of water exchange. In the following Section, the results of each calculation are presented and discussed in detail.

Tab. 3-1: Overview of BPW calculations

For each calculation the full GEM-Selektor record identification is provided together with the indication of the parameters varied and a short comment.

GEMS record id	Parameter varied	Remark
BPW_SIT:G:**ACW3a_BPW_03:1**:0:1:**25**:0:	Source case	ρ_b = 1'450 kg m^{-3}, pCO_2 = $10^{-2.83}$ bar
BPW_SIT:G:**ACW3a_BPW_03:2**:0:1:**25**:0:	100% = SOH distribution	= SOH sites entered generically as Ess,Esv, Esw
BPW_SIT:G:**ACW3a_BPW_03:3**:0:1:**25**:0:	ρ_b = 1'300 kg m^{-3}	Low bentonite compaction
BPW_SIT:G:**ACW3a_BPW_03:4**:0:1:**25**:0:	ρ_b = 1'600 kg m^{-3}	High bentonite compaction
BPW_SIT:G:**ACW3a_BPW_03:5**:0:1:**25**:0:	pCO_2 not fixed	Closed system (pco_2 unconstrained)
BPW_SIT:G:**ACW3a_BPW_03:6**:0:1:**25**:0:	log pCO2 = -2.2	SGT-2 reference value
BPW_SIT:G:**ACW3a_BPW_03:7**:0:1:**25**:0:	log pCO2 = -1.8	* SGT-2 highest value
BPW_SIT:G: exch_cycles_1000:R (Proc)	Water exchange cycles	Simulates evolution of BPW

* SGT-2 lowest value is log pCO_2 (bar) = -2.8, i.e. approximately the same value inferred for Bülach OPA water

[7] The term “source case” was preferred for these provisional calculations to “reference case”, which is reserved for the final BPW calculations presented in Chapter 4.

3.2 Discussion of BPW calculations

3.2.1 Source case

For the source case BPW calculation (25 °C, 1 bar), a bentonite dry bulk density of 1'450 kg m^{-3} was assumed. Further, the pCO_2 was constrained to $10^{-2.83}$ bar, the value corresponding to equilibrium with ACW3a as determined by chemical analysis. The "initial state" of the reacting MX-80 bentonite is given in Tab. 2-5 and the main results of the "source calculation" are shown in Tab. 3-2 (column 2) together with the initial compositions of reacting OPAw and MX-80 bentonite (column 1) and the differences between initial and final state (column 3), which facilitates the identification of the reactions involved during equilibration.

Tab. 3-2: Results of source case BPW calculations

	Initial state (ACW3a/MX-80)	**Final state (BPW/MX-80)**	**Difference (Final – Initial)**
T [°C]	25	25	0
p(tot) [bar]	1	1	0
log (pCO_2 [bar])	*-2.83*	-2.83	0
pH	7.28	7.41	0.13
Eh [V]	-0.204	-0.180	0.024
IS [mol/kgw]	0.510	0.586	0.076
MX-80 bentonite	*(mol)*	*(mol)*	
BaZ_2	5.00E-04	1.41E-07	-5.00E-04
CaZ_2	3.30E-02	3.42E-02	1.20E-03
KZ	1.30E-02	1.29E-02	-6.08E-05
MgZ_2	2.00E-02	1.99E-02	-1.05E-04
NaZ	6.68E-01	6.70E-01	2.33E-03
SrZ_2	2.00E-03	3.06E-04	-1.69E-03
Z^-(tot)	7.92E-01	7.92E-01	0
$= S^sOH_2^+$	2.10E-07	1.40E-06	1.19E-06
$= S^sOH$	6.50E-04	1.13E-03	4.83E-04
$= S^sO^-$	8.50E-04	3.66E-04	-4.84E-04
$= S^{w1}OH_2^+$	4.20E-06	2.79E-05	2.37E-05
$= S^{w1}OH$	1.30E-02	2.27E-02	9.66E-03
$= S^{w1}O^-$	1.70E-02	7.32E-03	-9.68E-03
$= S^{w2}OH_2^+$	9.40E-05	1.14E-03	1.04E-03
$= S^{w2}OH$	3.00E-02	2.92E-02	-7.69E-04
$= S^{w2}O^-$	3.00E-04	2.37E-05	-2.76E-04
= SOH(tot)	4.38E-02	5.54E-02	1.15E-02

Tab. 3-2: Cont.

	Initial state (ACW3a/MX-80)	Final state (BPW/MX-80)	Difference (Final – Initial)
Aqueous solution	(molality)	(molality)	
Al	-	1.67E-08	1.57E-08
Ba	-	1.47E-07	1.46E-07
C (inorganic)	8.42E-04	1.10E-03	2.62E-04
Ca	3.95E-02	2.77E-02	-1.18E-02
Cl	4.06E-01	4.04E-01	-1.34E-03
Fe	1.12E-12	1.25E-05	1.25E-05
K	1.93E-03	2.46E-03	5.35E-04
Mg	1.78E-02	1.87E-02	8.72E-04
Na*	5.04E-01	4.83E-01	-2.12E-01
S	2.84E-02	5.79E-02	2.96E-02
Si	-	1.78E-04	1.78E-04
Sr	3.13E-04	2.41E-04	-7.16E-05
Net charge (eq)	1.81E-02	6.53E-03	-1.15E-02
Gas	*(mol)*	*(mol)*	
CO_2	0.00E+00	7.24E-02	7.24E-02
CH_4	0.00E+00	8.77E-14	8.77E-14
H_2	0.00E+00	9.60E-08	9.60E-08
N_2	0.00E+00	4.85E+01	4.85E+01
O_2	0.00E+00	0.00E+00	0.00E+00
H_2S	0.00E+00	3.39E-09	3.39E-09
Solids	*Initial (mol)*	*Equilibrium (mol)*	
Baryte	1.00E-12	5.00E-04	5.00E-04
Calcite	3.00E-01	3.14E-01	1.36E-02
Pyrite	5.00E-01	5.04E-01	3.91E-03
Celestine	1.00E-12	1.70E-03	1.70E-03
Kaolinite	3.90E-02	3.90E-02	-1.00E-09
Gypsum	2.35E-02	1.01E-02	-1.34E-02
Siderite	8.60E-02	0.00E+00	-8.60E-02
Magnetite	4.30E-01	4.57E-01	2.74E-02
Quartz	1.66E+00	1.66E+00	-2.03E-05

* Na concentration includes Na^+ initially adsorbed on the (negatively charged) clay surface.

With respect to the initial OPAw, the equilibrated bentonite pore water is slightly more alkaline (pH increase from 7.28 to 7.41) and more saline (ionic strength increase from 0.51 m to 0.59 m). Most dissolved elemental concentrations change only to a minor extent. The major solution effects are a noticeable increase in sulphate and sodium concentrations and a decrease in calcium, the latter caused by uptake in the montmorillonite interlayer to compensate Sr displacement towards the aqueous solution. The uptake of calcium in the interlayer triggers significant gypsum dissolution, which is the reason of the increase in dissolved sulphate. On the other hand, the release of exchanged Ba, Sr and Ca from gypsum dissolution leads to precipitation of baryte celestine and calcite. The relatively high imposed pCO_2 ($10^{-2.83}$ bar) is achieved via CO_2 outgassing following the complete dissolution of siderite.

In Tab. 3-2, a net charge of +18.1 meq/kg clay is indicated for the aqueous OPAw solution. This charge arises from the assumed Na^+ excess on the clay surface compensating the negative charge generated by the surface hydroxyl groups' population. Summing up the charges of = SOH species leads to -18.1 meq/kg negative charge. This excess Na^+ is added to the native Na concentration of the OPAw to avoid generating an electrically charged initial system.[8] Upon equilibration, the net solution charge decreases to 6.5 meq/kg and the charge on the clay becomes correspondingly less negative (-6.5 meq/kg) implying an uptake of 11.5 mmol/kg protons from solution on the amphoteric surface sites (= SOH@ and SOH_2^+ species). The surface site protonation is a basic reaction, however leading to a final pH of the BPW only slightly higher than the initial pH of the ACW3a solution. This in turn indicates that counteracting acid reactions compensate to a large extent the effect of the protonation reactions. The pH-buffering mechanism is discussed more in detail in Section 3.2.2. The Eh is mainly controlled by the stability of iron-bearing phases. Under the prescribed conditions, siderite becomes unstable and the iron inventory is essentially transferred to magnetite and pyrite, which buffer the oxidation potential to low Eh, according to the explanations given in Section 3.2.6.

3.2.2 Effect of surface hydroxyl groups (= SOH) and pH buffering

In the previous source BPW calculation, the initial distribution of surface hydroxyl groups (= SOH) determined by Bradbury & Baeyens (2002) was assumed. Such initial state is based on the characterization of a few MX-80 samples and may not be representative of the bentonite that will be used in future as backfill material of the repository tunnels. It is therefore important to explore the effect of variations in the initial occupancies of the amphoteric surface sites, particularly considering their strong potential impact on *pH*. To this aim, a dedicated calculation was carried out, in which it was assumed that all amphoteric sites are initially occupied by neutral = SOH@ groups only, while both = SO^- and SOH_2^+ initial concentrations are assumed to be zero. Such a distribution is unrealistic, however useful as a test case to determine the sensitivity of the BPW model to large changes of the initial surface site occupancies. The effect of the modified initial protonation state is illustrated in Tab. 3-3. It is evident that the impact on pH, ionic strength and solution composition is minor, although with the new assumption a net proton release from the amphoteric surface sites to the aqueous solution is calculated, instead of an uptake as in the source calculation. The differences between final and initial = SOH(tot) values are +11.6 and -6.1 mmol/kg clay for the "source" and the "100% = SOH@ calculation", respectively, implying an excess of 17.6 mmol H^+ in the aqueous solution resulting from the latter calculation. Despite this large proton excess, the pH remains almost constant. Only a slight decrease from 7.41 to 7.38 is calculated, indicating again that buffering reactions must occur.

---

[8] Formally, this Na excess is assigned to the aqueous solution, which becomes then positively charged. The generation of charged pore water is an intrinsic feature of the 2SPNE SC/CE model. Because the 2SPNE SC/CE does not include an electrostatic term splitting the aqueous phase into of a charged diffuse double layer and an electrically neutral pore water, the opposite charge compensating the surface charge is uniformly distributed into a single homogeneous water phase, which is then in general not neutral.

Tab. 3-3: Results of BPW calculations: effect of surface hydroxyl speciation

	Initial state (ACW3a/MX-80) source case	**Final state (BPW/MX-80) source case**	**Initial state (ACW3a/MX-80) 100% = SOH@**	**Final state (BPW/MX-80) 100% = SOH@**
T [°C]	25	25	25	*25*
p(tot) [bar]	1	1	1	1
log (pCO_2 [bar])	*-2.83*	-2.83	*-2.83*	-2.83
pH	7.28	7.41	7.28	7.38
Eh [V]	-0.204	-0.180	-0.204	-0.179
IS [mol/kgw]	0.510	0.586	0.510	0.569
MX-80 bentonite	*(mol)*	*(mol)*	*(mol)*	*(mol)*
BaZ_2	5.00E-04	1.41E-07	5.00E-04	1.71E-07
CaZ_2	3.30E-02	3.42E-02	3.30E-02	4.16E-02
KZ	1.30E-02	1.29E-02	1.30E-02	1.29E-02
MgZ_2	2.00E-02	1.99E-02	2.00E-02	2.01E-02
NaZ	6.68E-01	6.70E-01	6.68E-01	6.55E-01
SrZ_2	2.00E-03	3.06E-04	2.00E-03	3.73E-04
Z^-(tot)	7.92E-01	7.92E-01	7.92E-01	7.92E-01
$= S^sOH_2^+$	2.10E-07	1.40E-06	0.00E+00	1.52E-06
$= S^sOH$	6.50E-04	1.13E-03	**1.50E-03**	1.15E-03
$= S^sO^-$	8.50E-04	3.66E-04	0.00E+00	3.47E-04
$= S^{w1}OH_2^+$	4.20E-06	2.79E-05	0.00E+00	3.04E-05
$= S^{w1}OH$	1.30E-02	2.27E-02	**3.00E-02**	2.30E-02
$= S^{w1}O^-$	1.70E-02	7.32E-03	0.00E+00	6.94E-03
$= S^{w2}OH_2^+$	9.40E-05	1.14E-03	0.00E+00	1.22E-03
$= S^{w2}OH$	3.00E-02	2.92E-02	**3.04E-02**	2.92E-02
$= S^{w2}O^-$	3.00E-04	2.37E-05	0.00E+00	2.21E-05
= SOH(tot)	4.38E-02	5.54E-02	6.19E-02	5.58E-02
Aqueous solution	(molality)	(molality)	(molality)	(molality)
Al	-	1.67E-08	-	1.56E-08
Ba	-	1.47E-07	-	1.61E-07
C (inorganic)	8.42E-04	1.10E-03	8.42E-04	1.03E-03
Ca	3.95E-02	2.77E-02	3.95E-02	3.09E-02
Cl	4.06E-01	4.04E-01	4.06E-01	4.05E-01
Fe	1.12E-12	1.25E-05	1.12E-12	1.39E-05
K	1.93E-03	2.46E-03	1.93E-03	2.40E-03

Tab. 3-3: Cont.

	Initial state (ACW3a/MX-80) source case	Final state (BPW/MX-80) source case	Initial state (ACW3a/MX-80) 100% = SOH@	Final state (BPW/MX-80) 100% = SOH@
Mg	1.78E-02	1.87E-02	1.78E-02	1.72E-02
Na*	5.04E-01	4.83E-01	5.04E-01	4.59E-01
S	2.84E-02	5.79E-02	2.84E-02	4.95E-02
Si	-	1.78E-04	-	1.78E-04
Sr	3.13E-04	2.41E-04	3.13E-04	2.69E-04
Net charge (eq)	1.81E-02	6.53E-03	0.00E+00	6.06E-03
Gas	*(mol)*	*(mol)*	*(mol)*	*(mol)*
CO_2	0.00E+00	7.24E-02	0.00E+00	7.28E-02
CH_4	0.00E+00	8.77E-14	0.00E+00	8.89E-14
H_2	0.00E+00	9.60E-08	0.00E+00	9.72E-08
N_2	0.00E+00	4.85E+01	0.00E+00	4.90E+01
O_2	0.00E+00	0.00E+00	0.00E+00	0.00E+00
H_2S	0.00E+00	3.39E-09	0.00E+00	3.43E-09
Solids	*Initial (mol)*	*(mol)*	*Initial (mol)*	*(mol)*
Baryte	1.00E-12	5.00E-04	1.00E-12	5.00E-04
Calcite	3.00E-01	3.14E-01	3.00E-01	3.13E-01
Pyrite	5.00E-01	5.04E-01	5.00E-01	5.08E-01
Celestine	1.00E-12	1.70E-03	1.00E-12	1.63E-03
Kaolinite	3.90E-02	3.90E-02	3.90E-02	3.90E-02
Gypsum	2.35E-02	1.01E-02	2.35E-02	2.68E-03
Siderite	8.60E-02	0.00E+00	8.60E-02	0.00E+00
Magnetite	4.30E-01	4.57E-01	4.30E-01	4.56E-01
Quartz	1.66E+00	1.66E+00	1.66E+00	1.66E+00

* Na concentration includes Na^+ initially adsorbed on the (negatively charged) clay surface. There is no such excess however in the "100% SOH@" calculation since a zero surface charge is assumed.

A detailed comparison of the results allowed us to identify the buffering mechanisms. It turns out that the complex interplay of dissolution/precipitation reactions of minor solids during the equilibration process is the main reason for the observed pH (and Eh) buffering. The dissolution of siderite releases aqueous Fe^{2+} that is then re-precipitated as pyrite and magnetite, according to the following reactions:

$$FeCO_3(s) + 2\ SO_4^{2-} + 16\ H^+ + 14\ e^- = FeS_2(s) + 8\ H_2O + CO_3^{2-}$$

$$3\ FeCO_3(s) + 4\ H_2O = Fe_3O_4(s) + 3\ CO_3^{2-} + 8\ H^+ + 2\ e^-$$

While the siderite to pyrite conversion is a basic reaction (protons consumption), the siderite to magnetite conversion produces acidity (protons release). These two simultaneous reactions therefore tend to buffer the pH. Combining and balancing the two reactions with the observed gypsum dissolution and calcite precipitation, and including carbonate/CO_2 equilibria, leads to the following combined reaction (CR):

$$22\ FeCO_3(s) + 2\ CaSO_4{*}H_2O = FeS_2(s) + 7\ Fe_3O_4(s) + 2\ CaCO_3(s) + 2\ H_2O + 20\ CO_2(g)$$

(siderite) (gypsum) (pyrite) (magnetite) (calcite)

The CR reaction largely controls the chemistry of the BPW. It is pH-dependent, although no protons or hydroxyl ions appear explicitly. As it proceeds to the right, CO_2 is degassed producing basicity and the pH rises. Conversely, if the reaction proceeds to the left carbonic acid is produced and the pH decreases. At fixed pCO_2, and provided that all five solids remain stable, the CR reaction is a pH buffer. In most cases considered in this report, however, the reaction proceeds to the right and the small siderite inventory dissolves completely.

In the SGT-2 model (Bradbury et al. 2014, Curti 2013) two BPW variants were calculated, corresponding to different treatments of carbonate/gas equilibria. In the "conventional" approach (also used in earlier BPW models) the pCO_2 was fixed via equilibrium with an external gas phase reacting with both Opalinus Clay and bentonite. This approach implies a physical connection with a large external gas reservoir and thus requires equilibration of CO_2 on the scale of geological formations via solute species diffusion. In contrast, the "novel" SGT-2 model (Berner et al. 2013, Bradbury et al., 2014) regards the bentonite as a system closed to gas exchange with external reservoirs. Carbonate species equilibrate only internally within the bentonite, there is no exchange with a gas phase.

The SGT-3 model presented here is somehow intermediate. It allows for equilibrium with a gas phase, however the CO_2 source is not external, but internal. The carbon dioxide is generated by the aforementioned CR and a prescribed pCO_2 is fixed by adding an appropriate amount of inert gas (N_2) to the gas phase. One may interpret this approach to be the most representative of near-field conditions, since the evolved CO_2 will mix with the (presumably chemically inert) H_2-rich gas generated through anaerobic Fe corrosion.

Note also that the CR also controls the Eh, since it involves balanced electron transfers among the Fe(II)/Fe(III) and sulphide/sulphate systems. Because siderite is consumed in the reaction, the Eh is finally buffered by the univariant pyrite-magnetite equilibrium (see Section 3.2.6 for details).

3.2.3 Effect of bentonite compaction ("porosity")

In this Section, the influence of different degrees of bentonite pre-compaction is examined. To this aim, the source case (ρ_b = 1'450 kg m^{-3}, $\varepsilon_{an,max}$ = 0.161) was compared with two calculations, in which the dry density was set to either to a lower or to a higher value as indicated in Tab. 2-7

(ρ_b = 1'300 kg m^{-3} and ρ_b = 1'600 kg m^{-3}, corresponding to $\varepsilon_{an,max}$ = 0.239 and 0.113, respectively). The results, summarized in Tab. 3-4, indicate only minor differences of exchanged ion populations, surface hydroxyl speciation, aqueous concentrations and mineral inventories in the three equilibrated BPWs. Therefore, one can conclude that the resulting BPW composition is remarkably stable within the bulk dry density range 1'300 – 1'600 kg m^{-3}. The only noticeable effect is a slight increase in ionic strength (from 0.57 m to 0.60 m) with increasing compaction. This is due to the decrease in the volume of external water as the degree of compaction increases. As a consequence, the total amount of Na^+ initially adsorbed on the clay (compensating the negative surface charge) is distributed over a smaller total volume of external water, so that Na-concentration and ionic strength increase.

Tab. 3-4: Results of BPW calculations: effect of bentonite compaction

	Initial state (ACW3a/MX-80) source case	**Final state (BPW/MX-80) low compaction 1'300 kg m^{-3}**	**Final state (ACW3a/MX-80) source case 1'450 kg m^{-3}**	**Final state (BPW/MX-80) high compaction 1'600 kg m^{-3}**
T [°C]	25	25	25	*25*
p(tot) [bar]	1	1	1	1
log (pCO_2 [bar])	*-2.83*	-2.83	-2.83	-2.83
pH	7.28	7.41	7.41	7.40
Eh [V]	-0.204	-0.180	-0.180	-0.180
IS [mol/kgw]	0.510	0.572	0.586	0.603
MX-80 bentonite	*(mol)*	*(mol)*	*(mol)*	*(mol)*
BaZ_2	5.00E-04	1.52E-07	1.41E-07	1.33E-07
CaZ_2	3.30E-02	3.70E-02	3.42E-02	3.23E-02
KZ	1.30E-02	1.29E-02	1.29E-02	1.30E-02
MgZ_2	2.00E-02	2.01E-02	1.99E-02	1.98E-02
NaZ	6.68E-01	6.64E-01	6.70E-01	6.74E-01
SrZ_2	2.00E-03	6.65E-04	3.06E-04	2.90E-04
Z^-(tot)	7.92E-01	7.93E-01	7.92E-01	7.92E-01
= $S^sOH_2^+$	2.10E-07	1.40E-06	1.40E-06	1.43E-06
= S^sOH	6.50E-04	1.13E-03	1.13E-03	1.14E-03
= S^sO^-	8.50E-04	3.66E-04	3.66E-04	3.61E-04
= $S^{w1}OH_2^+$	4.20E-06	2.80E-05	2.79E-05	2.85E-05
= $S^{w1}OH$	1.30E-02	2.27E-02	2.27E-02	2.27E-02
= $S^{w1}O^-$	1.70E-02	7.31E-03	7.32E-03	7.23E-03
= $S^{w2}OH_2^+$	9.40E-05	1.14E-03	1.14E-03	1.16E-03
= $S^{w2}OH$	3.00E-02	2.92E-02	2.92E-02	2.92E-02
= $S^{w2}O^-$	3.00E-04	2.37E-05	2.37E-05	2.33E-05
= SOH(tot)	4.38E-02	5.54E-02	5.54E-02	5.55E-02

Tab. 3-4: Cont.

	Initial state (ACW3a/MX-80) source case	Final state (BPW/MX-80) low compaction 1'300 kg m^{-3}	Final state (ACW3a/MX-80) source case 1'450 kg m^{-3}	Final state (BPW/MX-80) high compaction 1'600 kg m^{-3}
Aqueous solution	(molality)	(molality)	(molality)	(molality)
Al	-	1.66E-08	1.67E-08	1.65E-08
Ba	-	1.46E-07	1.47E-07	1.51E-07
C (inorganic)	8.42E-04	1.09E-03	1.10E-03	1.10E-03
Ca	3.95E-02	2.76E-02	2.77E-02	2.87E-02
Cl	4.06E-01	4.05E-01	4.04E-01	4.04E-01
Fe	1.12E-12	1.24E-05	1.25E-05	1.29E-05
K	1.93E-03	2.37E-03	2.46E-03	2.58E-03
Mg	1.78E-02	1.73E-02	1.87E-02	2.03E-02
Na*	5.04E-01	4.60E-01	4.83E-01	5.08E-01
S	2.84E-02	5.63E-02	5.79E-02	5.79E-02
Si	-	1.78E-04	1.78E-04	1.78E-04
Sr	3.13E-04	2.40E-04	2.41E-04	2.50E-04
Net charge (eq)	1.81E-02	3.46E-02	6.53E-03	8.82E-02
CO_2	0.00E+00	7.24E-02	7.24E-02	7.24E-02
CH_4	0.00E+00	8.77E-14	8.77E-14	8.76E-14
H_2	0.00E+00	9.60E-08	9.60E-08	9.59E-08
N_2	0.00E+00	4.85E+01	4.85E+01	4.85E+01
O_2	0.00E+00	0.00E+00	0.00E+00	0.00E+00
H_2S	0.00E+00	3.39E-09	3.39E-09	3.39E-09
Solids	*Initial (mol)*	*Equilibrium (mol)*	*Equilibrium (mol)*	*Equilibrium (mol)*
Baryte	-	5.00E-04	5.00E-04	5.00E-04
Calcite	3.00E-01	3.14E-01	3.14E-01	3.14E-01
Pyrite	5.00E-01	5.04E-01	5.04E-01	5.04E-01
Celestine	-	1.70E-03	1.70E-03	1.72E-03
Kaolinite	3.90E-02	3.90E-02	3.90E-02	3.90E-02
Gypsum	2.35E-02	1.01E-02	1.01E-02	1.13E-02
Siderite	8.60E-02	0.00E+00	0.00E+00	0.00E+00
Magnetite	4.30E-01	4.57E-01	4.57E-01	4.57E-01
Quartz	1.66E+00	1.66E+00	1.66E+00	1.66E+00

* Na concentration includes Na^+ initially adsorbed on the clay surface.

3.2.4 Effect of unconstrained pCO_2 (closed system)

In this Section, the source case is compared to an alternative calculation in which diffusion of CO_2 from or to a fictive gas reservoir (required to set a fixed pCO_2) is suppressed. This is equivalent as treating the saturated bentonite as a system closed to gas exchange, as in the "novel" BPW model variant (Berner et al. 2013, Bradbury et al. 2014) defined for SGT-2. Technically, this is achieved in GEM-Selektor by reducing the volume of gas phase to an infinitesimal amount, which has the advantage that the equilibrium pCO_2 can be easily read out from the output. The compared results from the two calculations are shown in Tab. 3-5.

It is anticipated that this calculation should yield a lower pH and a higher equilibrium pCO_2 because no CO_2 (i.e. no acidity) is allowed to escape from the aqueous solution. Indeed, the resulting pH is 6.9 (vs. 7.4 in the source calculation) and log (pCO_2 [bar]) is -1.77 (vs. -2.83). The dissolution/precipitation reactions are the same as in the open system, but mass transfer quantities are in general different. Notably, siderite is now dissolved only partially, i.e. it remains a stable phase. The aqueous composition does not change much, except for total carbonate (increase from 1.1 to 4.4 mM), sulphate (increase from 57.9 to 66.8 mM) and Ca (decrease from 27.7 to 23.7 mM). Due to the lower pH, the speciation of = SOH sites shifts towards enrichment of protonated species. The formerly negative clay surface becomes now slightly positively charged (+ 3.22 mmol/kgw, see net charge = -3.22 meq/kgw in the aqueous solution), implying a corresponding enrichment of Cl^- in the DDL layer. This result shows that the impact of the treatment of CO_2 equilibrium on the BPW calculations is much larger than the effect of bentonite compaction and initial distribution of protonated surface species.

Tab. 3-5: Results of BPW calculations: effect of unconstrained pCO_2

	Initial state (ACW3a/MX-80) source case	**Final state (ACW3a/MX-80) source case 1'450 kg m^{-3}**	**Final state (BPW/MX-80) closed system 1'450 kg m^{-3}**
T [°C]	25	25	*25*
p(tot) [bar]	1	1	1
log (pCO_2 [bar])	*-2.83*	-2.83	*-1.77*
pH	7.28	7.41	6.92
Eh [V]	-0.204	-0.180	-0.143
IS [mol/kgw]	0.510	0.586	0.575
MX-80 bentonite	*(mol)*	*(mol)*	*(mol)*
BaZ_2	5.00E-04	1.41E-07	1.33E-07
CaZ_2	3.30E-02	3.42E-02	3.24E-02
KZ	1.30E-02	1.29E-02	1.30E-02
MgZ_2	2.00E-02	1.99E-02	2.01E-02
NaZ	6.68E-01	6.70E-01	6.74E-01
SrZ_2	2.00E-03	3.06E-04	2.90E-04
Z^-(tot)	7.92E-01	7.92E-01	7.92E-01

Tab. 3-5: Cont.

	Initial state (ACW3a/MX-80) source case	Final state (ACW3a/MX-80) source case 1'450 kg m^{-3}	Final state (BPW/MX-80) closed system 1'450 kg m^{-3}
= $S^sOH_2^+$	2.10E-07	1.40E-06	5.13E-06
= S^sOH	6.50E-04	1.13E-03	1.35E-03
= S^sO^-	8.50E-04	3.66E-04	1.42E-04
= $S^{w1}OH_2^+$	4.20E-06	2.79E-05	1.03E-04
= $S^{w1}OH$	1.30E-02	2.27E-02	2.71E-02
= $S^{w1}O^-$	1.70E-02	7.32E-03	2.84E-03
= $S^{w2}OH_2^+$	9.40E-05	1.14E-03	3.25E-03
= $S^{w2}OH$	3.00E-02	2.92E-02	2.71E-02
= $S^{w2}O^-$	3.00E-04	2.37E-05	7.16E-06
= SOH(tot)	4.38E-02	5.54E-02	6.23E-02
Aqueous solution	(molality)	(molality)	(molality)
Al	-	1.67E-08	6.28E-09
Ba	-	1.47E-07	1.30E-07
C (inorganic)	8.42E-04	1.10E-03	4.40E-03
Ca	3.95E-02	2.77E-02	2.37E-02
Cl	4.06E-01	4.04E-01	4.05E-01
Fe	1.12E-12	1.25E-05	1.01E-04
K	1.93E-03	2.46E-03	2.31E-03
Mg	1.78E-02	1.87E-02	1.71E-02
Na	3.46E-01	4.83E-01	4.55E-01
S	2.84E-02	5.79E-02	6.68E-02
Si	-	1.78E-04	1.77E-04
Sr	3.13E-04	2.41E-04	2.06E-04
Net charge (eq)	1.81E-02	5.71E-02	-3.22E-03
Gas	*(mol)*	*(mol)*	*(mol)*
CO_2	0.00E+00	7.24E-02	-
CH_4	0.00E+00	8.77E-14	-
H_2	0.00E+00	9.60E-08	-
N_2	0.00E+00	4.85E+01	-
O_2	0.00E+00	0.00E+00	-
H_2S	0.00E+00	3.39E-09	-

Tab. 3-5: Cont.

	Initial state (ACW3a/MX-80) source case	Final state (ACW3a/MX-80) source case 1'450 kg m^{-3}	Final state (BPW/MX-80) closed system 1'450 kg m^{-3}
Solids	*Initial (mol)*	*Equilibrium (mol)*	*Equilibrium (mol)*
Baryte	-	5.00E-04	5.00E-04
Calcite	3.00E-01	3.14E-01	3.10E-01
Pyrite	5.00E-01	5.04E-01	5.00E-01
Celestine	-	1.70E-03	1.72E-03
Kaolinite	3.90E-02	3.90E-02	3.90E-02
Gypsum	2.35E-02	1.01E-02	1.59E-02
Siderite	8.60E-02	0.00E+00	7.56E-02
Magnetite	4.30E-01	4.57E-01	4.33E-01
Quartz	1.66E+00	1.66E+00	1.66E+00

* Na concentration includes Na^+ initially adsorbed on the clay surface.

3.2.5 Effect of different fixed pCO_2

The next variation illustrates the effect of setting different prescribed CO_2 partial pressures (Tab. 3-6). In the source calculation, a value of $10^{-2.83}$ bar, the same CO_2 partial pressure inferred to be in equilibrium with OPAw from the Bülach borehole, was assumed. The two fixed pCO_2 selected here for the sensitivity analysis are higher: $10^{-2.2}$ bar and $10^{-1.8}$ bar. They correspond to the reference and maximum CO_2 partial pressures assumed to be in equilibrium with BPW in the framework of SGT-2 safety assessment (Bradbury et al. 2014). The smallest pCO_2 assumed in SGT-2 ($10^{-2.5}$ bar) being larger than the present value in the source case, was therefore not considered. The results indicate the following chemical effects when increasing the pCO_2 from $10^{-2.8}$ to $10^{-1.8}$ bar:

- A pH decrease from 7.4 to 6.9, due to the progressively increasing amount of CO_2 produced by the buffering reaction remaining in the water.
- As pH decreases, the degree of protonation of amphoteric surface sites increases: [= SOH(tot)] increases from 55.4 to 62 mmol/kgw.
- As a consequence, the non-permanent surface charge increases and becomes even slightly positive at the highest pCO_2 (the bulk aqueous solution charge decreases from +57.1 to -1.2 mmol/kgw).
- Dissolved carbonate, sulphate and iron increase, whereas calcium decreases.

The amounts of dissolved gypsum and precipitated calcite increase slightly.

Tab. 3-6: Results of BPW calculations: effect of different pCO_2

	Initial state (ACW3a/MX-80) source case	**Final state (ACW3a/MX-80) source case log(pCO_2) = -2.8**	**Final state (ACW3a/MX-80) variation 1 log(pCO_2) = -2.2**	**Final state (ACW3a/MX-80) variation 2 log(pCO_2) = -1.8**
T [°C]	25	25	25	*25*
p(tot) [bar]	1	1	1	1
log (pCO_2 [bar])	*-2.83*	-2.83	-2.20	-1.80
pH	7.28	7.41	7.12	6.94
Eh [V]	-0.204	-0.180	-0.159	-0.144
IS [mol/kgw]	0.510	0.586	0.578	0.575
MX-80 bentonite	*(mol)*	*(mol)*	*(mol)*	*(mol)*
BaZ_2	5.00E-04	1.41E-07	1.36E-07	1.33E-07
CaZ_2	3.30E-02	3.42E-02	3.31E-02	3.24E-02
KZ	1.30E-02	1.29E-02	1.30E-02	1.30E-02
MgZ_2	2.00E-02	1.99E-02	2.00E-02	2.01E-02
NaZ	6.68E-01	6.70E-01	6.72E-01	6.73E-01
SrZ_2	2.00E-03	3.06E-04	2.96E-04	2.91E-04
Z^-(tot)	7.92E-01	7.92E-01	7.92E-01	7.92E-01
= $S^sOH_2^+$	2.10E-07	1.40E-06	3.06E-06	4.91E-06
= S^sOH	6.50E-04	1.13E-03	1.28E-03	1.35E-03
= S^sO^-	8.50E-04	3.66E-04	2.14E-04	1.47E-04
= $S^{w1}OH_2^+$	4.20E-06	2.79E-05	6.12E-05	9.82E-05
= $S^{w1}OH$	1.30E-02	2.27E-02	2.57E-02	2.70E-02
= $S^{w1}O^-$	1.70E-02	7.32E-03	4.28E-03	2.95E-03
= $S^{w2}OH_2^+$	9.40E-05	1.14E-03	2.13E-03	3.14E-03
= $S^{w2}OH$	3.00E-02	2.92E-02	2.83E-02	2.72E-02
= $S^{w2}O^-$	3.00E-04	2.37E-05	1.18E-05	7.48E-06
= SOH(tot)	4.38E-02	5.54E-02	5.96E-02	6.20E-02
Aqueous solution	(molality)	(molality)	(molality)	(molality)
Al	-	1.67E-08	9.19E-09	6.48E-09
Ba	-	1.47E-07	1.36E-07	1.30E-07
C (inorganic)	8.42E-04	1.10E-03	2.47E-03	4.19E-03
Ca	3.95E-02	2.77E-02	2.51E-02	2.38E-02
Cl	4.06E-01	4.04E-01	4.04E-01	4.04E-01
Fe	1.12E-12	1.25E-05	4.23E-05	9.34E-05

Tab. 3-6: Cont.

	Initial state (ACW3a/MX-80) source case	Final state (ACW3a/MX-80) source case $log(pCO_2) = -2.8$	Final state (ACW3a/MX-80) variation 1 $log(pCO_2) = -2.2$	Final state (ACW3a/MX-80) variation 2 $log(pCO_2) = -1.8$
K	1.93E-03	2.46E-03	2.37E-03	2.31E-03
Mg	1.78E-02	1.87E-02	1.77E-02	1.72E-02
Na*	5.04E-01	4.83E-01	4.65E-01	4.55E-01
S	2.84E-02	5.79E-02	6.32E-02	6.65E-02
Si	-	1.78E-04	1.77E-04	1.77E-04
Sr	3.13E-04	2.41E-04	2.18E-04	2.07E-04
Net charge (eq.)	1.81E-02	5.71E-02	2.02E-02	-1.22E-03
Gas	*(mol)*	*(mol)*	*(mol)*	*(mol)*
CO_2	0.00E+00	7.24E-02	7.02E-02	6.89E-02
CH_4	0.00E+00	8.77E-14	1.77E-14	6.38E-15
H_2	0.00E+00	9.60E-08	1.49E-08	4.54E-09
N_2	0.00E+00	4.85E+01	1.11E+01	4.30E+00
O_2	0.00E+00	0.00E+00	0.00E+00	0.00E+00
H_2S	0.00E+00	3.39E-09	6.82E-10	2.46E-10
Solids	*(mol)*	*(mol)*	*(mol)*	*(mol)*
Baryte	-	5.00E-04	5.00E-04	5.00E-04
Calcite	3.00E-01	3.14E-01	3.16E-01	3.17E-01
Pyrite	5.00E-01	5.04E-01	5.04E-01	5.04E-01
Celestine	-	1.70E-03	1.71E-03	1.72E-03
Kaolinite	3.90E-02	3.90E-02	3.90E-02	3.90E-02
Gypsum	2.35E-02	1.01E-02	9.47E-03	9.09E-03
Siderite	8.60E-02	0.00E+00	0.00E+00	0.00E+00
Magnetite	4.30E-01	4.57E-01	4.57E-01	4.57E-01
Quartz	1.66E+00	1.66E+00	1.66E+00	1.66E+00

* Na concentration includes Na^+ initially adsorbed on the clay surface.

It is important to note that the results of the calculation carried out by fixing pCO_2 at $10^{-1.8}$ bar are very similar to those obtained for the "closed system" calculation without separate gas phase. This is not surprising, since in the latter case the calculated equilibrium pCO_2 ($10^{-1.77}$ bar) is very close to $10^{-1.8}$ bar. This equivalence of results, though coincidental, is nevertheless useful, since it mitigates the dilemma, whether one should use constrained or unconstrained pCO_2 conditions for the calculations of BPWs. Closed system conditions can be reasonably well simulated by fixing the pCO_2 at the highest value estimated for Opalinus Clay conditions in SGT-2.

3.2.6 Control of oxidation potential (Eh) through iron phases

This Section explains how the oxidation potential (Eh) is controlled in the present BPW model. Following previous BPW models, it is assumed that Eh is essentially determined by the Fe(II)-Fe(III) and sulphate/sulphide systems, specifically through Fe solids coexisting at equilibrium with the pore solution. In MX-80 bentonite, an initial assemblage of minor Fe-minerals has been determined through the previously cited characterization studies, including siderite, pyrite and Fe oxy-hydroxide phases (Bradbury & Baeyens 2002). Moreover, it is further assumed that the pore solution will always be in equilibrium with magnetite (Fe_3O_4), which will be present in large excess as canister corrosion product.

Recent analyses on samples from the FEBEX and ABM2 field experiments have revealed the presence of both primary and secondary Fe(II) and Fe(III) minerals in MX-80 bentonite after prolonged interaction with steel at elevated temperature, confirming the reactivity of the iron redox system (Hadi et al. 2017, Hadi et al. 2019, Jenni et al. 2019). In the ABM2 experiments, synthetic granitic water was circulated at 130 °C during up to 5 years, while in the FEBEX experiments the interaction proceeded at 100 °C under non-saturated conditions with variable humidity during 18 years. In both cases, goethite was formed as main corrosion product, however in a limited oxidized region assigned to an initial transient phase of aerobic corrosion. In other regions of the steel/bentonite interface Fe(II) enrichment was detected, arising from later anaerobic corrosion after consumption of the initial oxygen. In the ABM2 samples, siderite and magnetite were identified in this region as secondary corrosion products.

The PSI-Nagra database includes selected thermodynamic data for common low-temperature Fe-solids, such as siderite ($FeCO_3$), pyrite (FeS_2), melanterite ($FeSO_4 \cdot 7H_2O$), hematite (Fe_2O_3), magnetite (Fe_3O_4), ferrihydrite, $Fe(OH)_3$*nH_2O and goethite (FeOOH). These are the phases that may constrain, together with pH, the oxidation potential in the modelled BPW system. It is possible to obtain an overview of Eh-pH relations for the BPW system based on relatively simple Eh-pH diagrams within the system Fe-O-H-S-C. To this aim, calculations were carried out with Phreeplot (Kinniburgh and Cooper, 2004). This software iterates PhreeqC to construct Eh-pH stability diagrams, using either the default or any user-defined thermodynamic database complying with the PhreeqC format. In this case, we used the available PhreeqC version of PSI-Nagra database.

In Fig. 3-1a,b,c three such Eh-pH diagrams are shown. The first two (a, b) closely reflect the aqueous composition calculated for the source BPW, i.e. they assume fixed Na, Cl, C, S, Fe aqueous concentrations similar to those calculated at equilibrium by applying the GEM-Selektor BPW model. The third diagram (c) assumes a 5 times higher carbonate concentration. The source case calculation corresponds to case (b), in which goethite was excluded on purpose from equilibrium. For the stable final Fe-phase assemblage pyrite-magnetite (see Tab. 3-2) the Phreeplot calculation predicts a reducing Eh of about -200 mV, which is consistent with the results of GEM-Selektor. In the Eh-pH diagram (b) siderite does not appear because it is unstable under these conditions. This is as well in agreement with the results of the “source case” GEM-Selektor calculation, which predicts complete dissolution of siderite upon equilibration. When the concentration of carbonate is raised by a factor 5, as assumed for the calculations leading to diagram (c), a siderite stability region between the magnetite and pyrite stability areas appears.

The calculation for the Eh-pH diagram (a) was carried assuming the same fixed concentrations as in case (b). The only difference was that also goethite was included in the selection of Fe-phases susceptible to reach equilibrium. The result shows that goethite, instead of magnetite (or at higher Eh ferrihydrite), is predicted to be the stable Fe-solid in the oxidizing region of the Eh-pH diagram. In this case the equilibrium conditions of the BPW system run along the univariant pyrite-goethite equilibrium line. Compared to the source case (b), the corresponding

GEM-Selektor calculation (not tabulated here) yields a similar BPW composition, with pH ≈ 7.5, I = 0.53 m and an even lower Eh (-275 mV). Thus, including or excluding goethite causes only minor differences in the calculated BPW composition and characteristics.

Goethite is in the present and preliminary calculations excluded as potentially precipitating phase based on the following arguments:

(I) The updated thermodynamic database TDB2020, which will be used for the definitive BPW calculations (see Chapter 4), includes a thorough revision of Fe data based on the NEA reviews. The revised solubility product of goethite data will be more than one order of magnitude higher (it will change from $\log^*K_{s,0}$ = -1.0 to +0.33) implying a significantly higher solubility. Consequently, it is expected that goethite will no longer be stable in the final BPW calculations. The stability field of goethite in Fig. 3-1a will shrink and presumably a magnetite stability field in equilibrium with pyrite will appear.

(II) Formation of goethite detected in field experiments during bentonite/steel interaction seems to be related exclusively to the transient initial aerobic phase of steel corrosion (Hadi et al. 2017, Hadi et al. 2019, Jenni et al. 2019). Under the anaerobic conditions representative of the long-term evolution, siderite and magnetite were detected as stable secondary solids.

(III) There is experimental evidence that goethite is not stable under any condition at near-neutral pH. The studies of Schwertmann et al. (2004) and Cudennec & Lecerf (2006) clearly show that the first solid precipitating upon oxidation of Fe(II) aqueous solutions is usually ferrihydrite, $Fe^{III}(OH)_3{}^*nH_2O$. At low temperatures, this metastable, poorly crystalline phase transforms slowly either to goethite or hematite, depending on pH. Formation of goethite requires either alkaline or acidic conditions, whereas at near-neutral conditions predicted for BPW (pH 7 – 8) it does not form. Under such conditions, hematite (α-Fe_2O_3) is the crystalline phase observed as end-product of ferrihydrite[9].

[9] Note that in the Eh-pH diagrams shown in Fig. 3-1 hematite does not appear because it was excluded in the Phreeplot calculations, in order to emphasize short-term conditions.

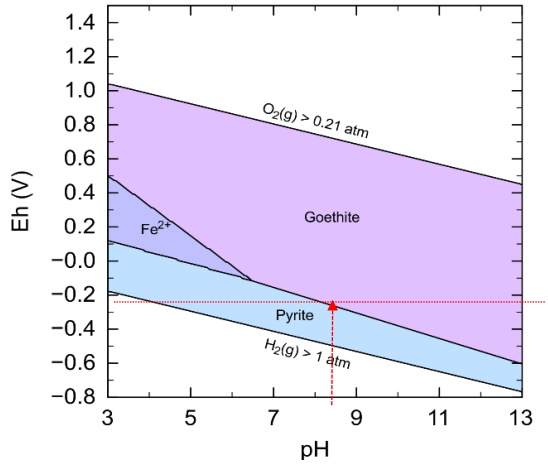

(a) all Fe minerals included

[Fe] = 2.0×10^{-5} m
[S] = 5.8×10^{-2} m
[C] = 1.1×10^{-3} m
[NaCl] = 0.4 m

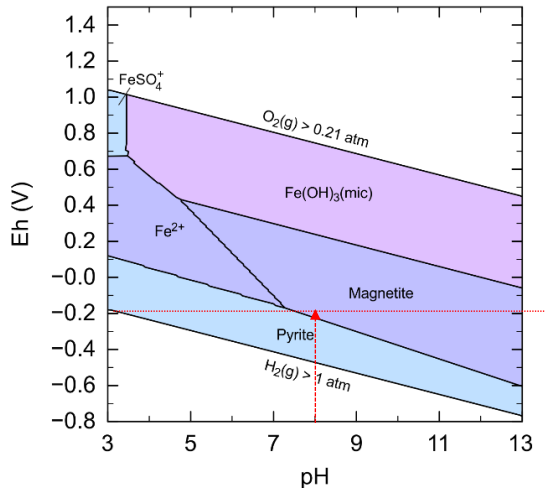

(b) goethite out

[Fe] = 2.0×10^{-5} m
[S] = 5.8×10^{-2} m
[C] = 1.1×10^{-3} m
[NaCl] = 0.4 m

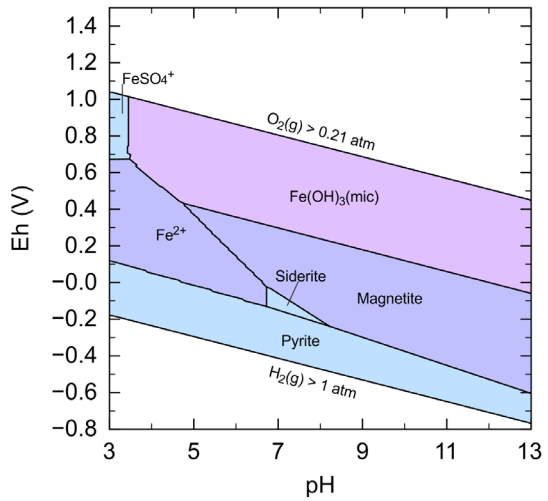

(c) goethite out, high carbonate

[Fe] = 2.0×10^{-5} m
[S] = 5.8×10^{-2} m
[C] = 5.0×10^{-3} m
[NaCl] = 0.4 m

Fig. 3-1: Eh-pH diagrams for BPW conditions at 25 °C and 1 bar

The three variants reflect different assumptions in aqueous concentrations or phase selection. See text for explanations.

3.2.7 Chemical evolution of the bentonite pore water

The model as applied so far calculates the initial stage of the BPW evolution, i.e. a "single pass" reaction in which the first batch of OPA pore water saturating the external porosity reacts with intact bentonite. Under repository conditions, the aqueous phase will penetrate slowly from outside into the bentonite buffer as it saturates it. The composition of this waterfront will progressively evolve as it continuously reacts with pristine bentonite. This situation is similar to that in a column experiment: the initial pore water is flushed through a long section of intact porous solid material and evolves in composition as it reacts with an increasing amount of intact solid material. Conversely, if one focuses on a small portion of bentonite at the upstream boundary of the column (i.e. the external boundary of bentonite), this (immobile) portion of solid will continuously react with new volume batches of pristine Opalinus Clay pore water. Both BPW and bentonite compositions will vary as a function of the total volume of OPAw that has reacted until the exchanged cation population and mineral inventories are in equilibrium with the intruding OPAw. This situation is similar to a leach experiment, in which a large volume of aqueous phase with constant composition is continuously passed over a limited amount of solid "sample".

Both situations that we will call shortly "flush" and "leach" scenarios can be modelled with the help of the GEM-Selektor's GEM2MT module. With this module, sequential reactors are implemented, providing a simple representation of BPW evolution as a function of space and "time" as schematically shown in Fig. 3-2. The space is simulated as a number of equivalent boxes ("nodes") in which a given amount of fluid entering on the left side reacts with a batch of solid (bentonite in this case). The reacted water volume is subsequently transferred to the next node with intact bentonite on the right and so on until it reaches the final node at the end of exchange cycle 1. A new cycle then starts (i.e. a new "time" step), taking into account the previously recorded changes in bentonite composition (i.e. exchanged ion populations and solid inventories). Although not a true reactive transport calculation, sequential reactors provide a simple mean to simulate system evolution as a function of space and time and provide boundary compositions of the bentonite pore waters.

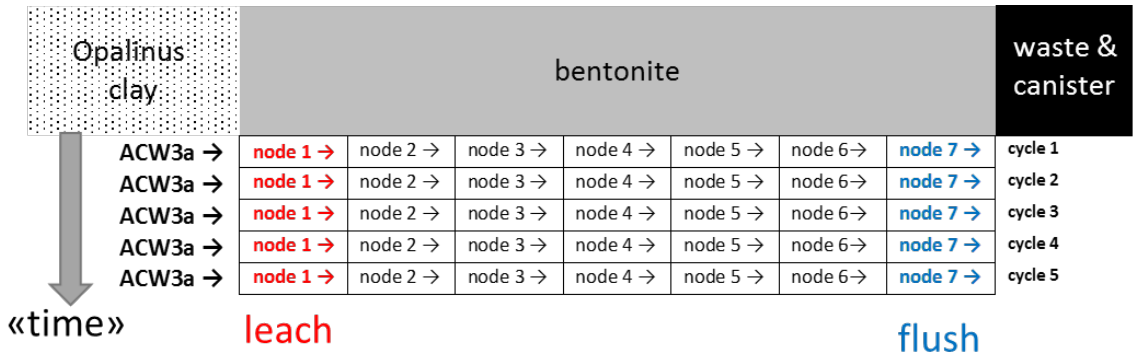

Fig. 3-2: Principle of sequential reactor provided in the GEM2MT module as applied to the BPW evolution

Calculations were performed only for the "closed system" model to avoid complications related to constrained pCO_2 conditions. The bentonite column was discretized in 20 nodes, each containing 1 kg of dry MX-80 bentonite. The solid in node 1 is brought in contact with 0.1411 kg of pristine ACW3a water, which corresponds to the S/W ratio assumed in the source BPW calculation.

Fig. 3-3 shows selected results obtained for 1'000 exchange cycles at node 1 (leach scenario, external bentonite boundary). Only the essential data are shown: the evolution of Na and Ca in pore water, of exchanged cations in the montmorillonite interlayer and the mole amounts of key reactive minerals (calcite, celestine, gypsum pyrite, magnetite and siderite) as well as Eh and pH. The ionic strength remains remarkably constant (0.502 to 0.543 m). The model predicts complete dissolution of the initial inventories of gypsum, celestine and siderite after 2, 95 and 297 water exchange cycles, respectively. The dissolution of siderite is triggered by precipitation of magnetite and pyrite. The increase in pyrite is barely visible in the plot because of the large initial inventory compared to siderite.

The release of carbonate from the dissolving siderite does not lead to precipitation of calcite. On the contrary, slight dissolution of calcite is observed. This apparently contradictory behaviour can be readily explained by noting that a noticeable amount of Ca is exchanged for Na during the first 100 cycles. The displacement of dissolved Ca to the interlayer prevents calcite precipitation, in spite of the increase in total dissolved carbonate.

After about 100 exchange cycles the Na and Ca molalities become equal to the concentrations in the pristine ACW3a water, indicating that the exchanged cation populations in the clay have reached equilibrium with the ACW3a water.

After complete dissolution of siderite, the pH rises from 6.8 to 7.3, which triggers an Eh decrease from -136 to -177 mV. This pH-Eh behaviour is explained by the Eh-pH diagrams shown in Fig. 3-1. As long as siderite coexists with magnetite and pyrite both pH and Eh are fixed at constant values determined by the Fe, sulphate and carbonate concentrations specific to the system (e.g. triple point siderite-magnetite-pyrite in Fig. 3-1b). Once siderite is dissolved, pH and Eh values are free to “move” along the univariant magnetite-pyrite equilibrium line. It is evident that an Eh decrease must follow from an increase in pH.

The analyses of results from GEM2MT calculations for nodes 10 and 20, which represents the BPW the middle and downstream boundary of the modelled bentonite buffer, indicate a similar evolution as for the upstream bentonite boundary (node 1), but the processes are delayed (onset at higher exchange cycle number). In all cases, one ends up with a final BPW water composition at the end of the calculated 1000 exchange cycles, which is – not surprisingly - almost identical to the reacting ACW3a water. This end-of-cycles composition is summarized in Tab. 3-6. The only noticeable differences with respect to the pristine ACW3a water are the concentrations of carbonate and of elements that were not included in the ACW3a model (Ba, Fe, Al, Si) but are considered in the BPW model. The concentrations of the cited elements are controlled by the mineral inventory in bentonite. This water can be taken to represent “mature” BPW anywhere within the bentonite buffer, under conditions closed to CO_2 exchange.

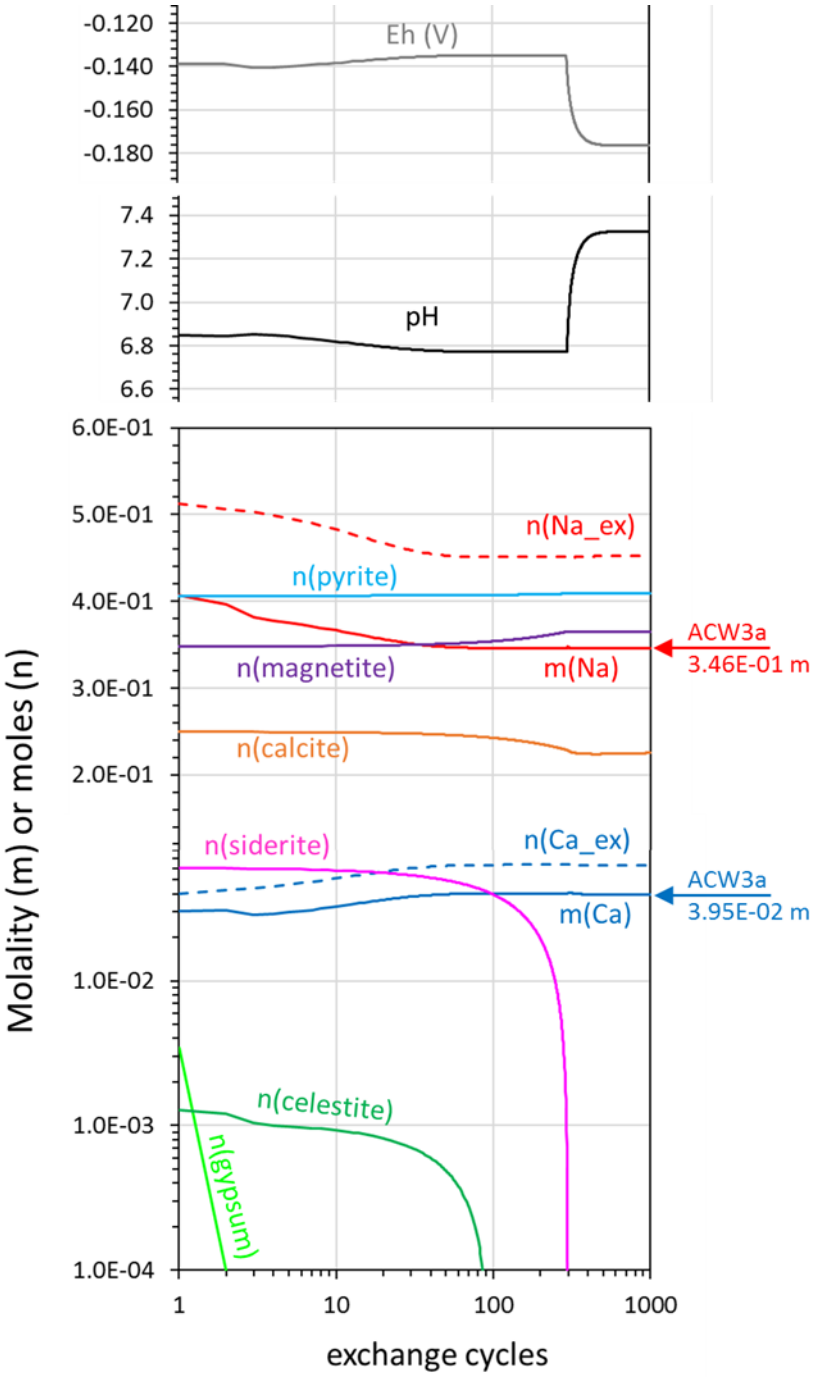

Fig. 3-3: Calculated evolution of BPW as a function of water exchange cycles at the external interface of MX80 bentonite

The arrows indicate the initial molalities of Ca and Na in ACW3a water.

Tab. 3-6: Results of BPW sequential reactor calculations (ρ_{dry} = 1'450 kg m^{-3} and closed system) after 1 and 1'000 water exchange cycle

	Initial state (ACW3a/MX-80)	**Cycle 1 Closed system 1'450 kg m^{-3}**	**Cycle 1000 Closed system 1'450 kg m^{-3}**
T [°C]	25	25	25
p(tot) [bar]	1	1	1
log (pCO_2 [bar])	*-2.83*	-	-
pH	7.28	6.86	7.33
Eh [V]	-0.204	-0.140	-0.177
IS [mol/kgw]	0.510	0.543	0.510
MX-80 bentonite	*(mol)*	*(mol)*	*(mol)*
BaZ_2	5.00E-04	1.52E-07	3.04E-07
CaZ_2	3.30E-02	3.70E-02	6.27E-02
KZ	1.30E-02	1.04E-02	9.52E-03
MgZ_2	2.00E-02	1.67E-02	2.48E-02
NaZ	6.68E-01	5.19E-01	4.52E-01
SrZ_2	2.00E-03	3.32E-04	5.10E-04
Z^-(tot)	7.92E-01	7.92E-01	7.92E-01
Aqueous solution	(molality)	(molality)	(molality)
Al	-	5.64E-09	1.38E-08
Ba	-	1.52E-07	2.26E-07
C (inorganic)	8.42E-04	3.92E-03	8.20E-04
Ca	3.95E-02	2.89E-02	3.95E-02
Cl	4.06E-01	4.05E-01	4.06E-01
Fe	-	1.23E-04	1.65E-05
K	1.93E-03	2.20E-03	1.93E-03
Mg	1.78E-02	1.51E-02	1.78E-02
Na	3.46E-01	4.16E-01	3.46E-01
S	2.84E-02	5.00E-02	2.84E-02
Si	-	1.77E-04	1.78E-04
Sr	3.13E-04	2.52E-04	3.13E-04
Net charge (eq)	1.81E-02	-1.95E-03	6.17E-09

Tab. 3-6: Cont.

	Initial state (ACW3a/MX-80)	Cycle 1 Closed system 1'450 kg m^{-3}	Cycle 1000 Closed system 1'450 kg m^{-3}
Solids	*(mol)*	*(mol)*	*(mol)*
Baryte	-	4.02E-04	3.77E-04
Calcite	2.42E-01	2.50E-01	2.25E-01
Pyrite	4.03E-01	4.06E-01	4.09E-01
Celestine	-	1.30E-03	0
Kaolinite	3.14E-02	3.14E-02	3.14E-02
Gypsum	1.89E-02	3.43E-03	0
Siderite	6.92E-02	6.04E-02	0
Magnetite	3.46E-01	3.48E-01	3.65E-01
Quartz	1.34E+00	1.34E+00	1.32E+00

Note: The initial inventories of minerals are somewhat lower than in the previous calculations due to a slightly different setup in the input file. Moreover, by comparing the cycle 1 results with the corresponding results in Tab. 3-5 (rightmost column) minor differences are evident. These are due to the fact that in the exchange cycles calculations no Na+/Cl- was introduced to balance the surface charge of the clay.

4 Final BPW calculations (TDB 2020)

4.1 Transfer of model to TDB 2020

All calculations presented so far serve to illustrate the development of the BPW model and have been carried out using the now outdated PSI-Nagra TDB 12/07, which has been recently updated to TDB 2020 (Hummel & Thoenen, 2022). Moreover, BPWs have been computed using a preliminary Opalinus Clay Water derived from data obtained from the Bülach borehole. This water has the highest salinity measured among all waters extracted so far from borehole samples, is outside the selected repository perimeter of the selected site at Stadel (Nördlich Lägern) and is thus not representative.

In this chapter, updated BPW calculations referring to the selected site at Nördlich Lägern, to be used for tasks related to the safety assessment (e.g. radionuclide solubility limits and sorption coefficients determination), are presented and the results briefly discussed. The calculations have all been carried out using a new GEM-Selektor version (v. 3.9.0) and TDB2020, following a methodology consistent with that used to define the reacting Opalinus Clay Waters (see next Section).

For all BPW calculations, the same initial state of the clay/water system as indicated in the former "source calculation" are used (Tab. 3-2). Only the composition of the reacting OPAw changes in the input files. This means that the same initial exchanged cations and amphoteric sites populations specified in Tab. 3-2 (arising from the characterization work of Bradbury & Baeyens 2002) are used to define the initial state of the clay. In all cases 1 kg of MX-80 bentonite compacted to 1'450 kg m^{-3} dry density reacts with 1141 g of a specific new OPAw. The amount of reacting water corresponds to the maximum anion porosity determined for that dry density according to the empirical equations of Van Loon (2013) (16.1%, see Tab. 2-6).

4.2 Definition of Opalinus Clay Waters (OPAw)

Mäder & Wersin (2022) have defined three provisional in-situ Opalinus Clay pore waters for a potential repository site in the Nördlich Lägern (NL) and Zürich Nordost (ZNO) perimeters. The data available at the time of this reporting indicate that these waters have a salinity intermediate between the Bülach pore water from the boundary region of Nördlich Lägern (NL) and the low salinity waters extracted from Jura-Ost (JO) borehole samples. Because the definitive Opalinus Clay waters were just released in late 2022, in agreement with Nagra it was decided to use the defined NL-ZNO in-situ waters to compute the final BPWs. The processing of the extensive pore water data obtained from the deep drilling campaign has shown that pore waters from Zürich Nordost and Nördlich Lägern are rather identical (except for the high-salinity pore water from Bülach). Therefore, a common OPA reference pore water has been defined for these two regions (see Mäder & Wersin 2022). In addition to the NL-ZNO pore water, BU also released a revised version of the Bülach pore water, which is used here to define a high-salinity BPW variant. Finally, on Nagra's request two artificial OPAw are defined here to explore the sensitivity of the calculated BPW compositions and characteristics on realistic salinity variations.

The released in-situ OPAw from BU were all computed at 25 °C and 1 bar total pressure assuming the same externally imposed CO_2 partial pressures ($10^{-2.8}$, $10^{-2.2}$ and $10^{-1.8}$ bar) as in SGT-2 (Bradbury et al. 2014) and saturation equilibria with a number of minor minerals (calcite, dolomite, quartz, celestine, siderite, pyrite, fluorite, kaolinite, barite and rhodochrosite). For the final BPW calculations, the BU Opalinus Clay waters were first recalculated with GEM-Selektor v. 3.9.0/TDB2020 using the SIT activity model. In order to keep as far as possible methodological

consistency, the same pCO_2 values and saturation equilibria were assumed in both types of water, however with the addition of magnetite equilibrium in the BPW calculations to represent the canister corrosion products.

The adjusted GEM-Selektor OPAw are shown in Tab. 4-1, together with the original BU waters. The results indicate that compositional modifications due to the "transfer procedure" are minor except for Fe aqueous concentrations, which are up to one order of magnitude lower when calculated with GEM-Selektor v. 3.9.0/TDB2020. In the latter calculations siderite is not stable at the required Eh and pH and replaced by magnetite in equilibrium with pyrite. This issue is discussed in detail in Appendix 3. It turns out that the discrepancies in the Fe concentrations are not related to the revision of Fe data involved in the TDB2020 update (Hummel & Thoenen 2022), but by the omission of magnetite as potential equilibrium phase in the PHREEQC input of BU. Indeed, the OPAw water as supplied by BU is strongly oversaturated with respect to magnetite (as defined in TDB2020) and thus apparently treated as kinetically inhibited solid.

Tab. 4-1: Opalinus Clay in-situ pore waters from the NL-ZNO regions: original compositions from Bern University (BU) compared to compositions adjusted using GEM-Selektor at PSI

Calc. ID Implementor	**OPAw_NL-ZNO-28**		**OPAw_NL-ZNO-22**		**OPAw_NL-ZNO-18**	
	BU	**PSI**	**BU**	**PSI**	**BU**	**PSI**
log $p(CO_2)$/bar	-2.80	-2.79	-2.20	-2.20	-1.80	-1.80
pH	7.40	7.40	7.10	7.10	6.90	6.90
pe	-3.00	-3.22	-2.66	-2.83	-2.43	-2.58
Eh	-0.178	-0.190	-0.157	-0.167	-0.144	-0.152
IS /m	0.312	0.317	0.313	0.319	0.314	0.321
Molality						
Al	1.41E-08	2.13E-08	8.61E-09	2.09E-08	9.26E-09	2.86E-08
Ba	1.56E-07	1.56E-07	1.57E-07	1.57E-07	1.57E-07	1.58E-07
C(IV)	1.02E-03	1.07E-03	2.12E-03	2.21E-03	3.54E-03	3.68E-03
Ca	2.01E-02	2.01E-02	2.02E-02	2.03E-02	2.04E-02	2.05E-02
Cl	0.240	0.239	0.240	0.240	0.240	0.241
F	1.33E-04	1.74E-04	1.33E-04	1.74E-04	1.32E-04	1.74E-04
Fe	**8.45E-05**	**7.14E-06**	**8.63E-05**	**2.56E-05**	8.85E-05	5.95E-05
K	2.13E-03	2.13E-03	2.13E-03	2.13E-03	2.14E-03	2.14E-03
Mg	1.53E-02	1.43E-02	1.55E-02	1.45E-02	1.56E-02	1.46E-02
Mn	5.64E-05	8.16E-05	5.74E-05	8.24E-05	5.86E-05	8.33E-05
Na	0.213	0.215	0.214	0.215	0.214	0.216
S(VI)	2.29E-02	2.29E-02	2.29E-02	2.29E-02	2.29E-02	2.29E-02
Si	1.78E-04	1.73E-04	1.77E-04	1.72E-04	1.77E-04	1.72E-04
Sr	2.70E-04	3.67E-04	2.71E-04	3.70E-04	2.73E-04	3.73E-04

Tab. 4-2 shows an analogous comparison for the revised Bülach porewater and the two artificial low-salinity (OPAw_NL-ZNO_ls) and high-salinity (OPAw_NL-ZNO_hs) Opalinus Clay waters. The artificial waters were generated simply by first subtracting/adding NaCl to reach limiting ionic strengths of 0.15 m and 1.0 m, respectively, from OPAw_NL-ZNO-22, then recalculating thermodynamic equilibrium without any further re-adjustments of pH, Eh or pCO_2. An ionic strength of 0.15 m corresponds to the lowest salinities measured so far in waters extracted from JO borehole samples, whereas the IS = 1.0 m is slightly above the estimated maximum ionic strength of Opalinus Clay porewater ("Mt. Russelin" variant, IS = 0.8 m, see Tab. 6-3 in Mäder 2009). The purpose of these waters is to explore the potential effects of realistic salinity variations in OPAw on composition and characteristics of the BPWs (sensitivity analysis). As for the pore waters reported in Tab. 4-1, the only significant discrepancy between BU and PSI versions of the OPAw from Bülach is the calculated Fe concentration, which is 13 times lower in the PSI version. Also in this case, siderite is calculated to be undersaturated and the Fe concentration is controlled by pyrite and magnetite.

Tab. 4-2: Opalinus Clay in-situ pore water from the Bülach-1 borehole and two artificial low-salinity and high salinity pore waters derived from OPAw_NL-ZNO-22

Calc. ID Implementor	**OPAw_BUL-28**		**OPAw_NL-ZNO-ls**	**OPAw_NL-ZNO-hs**
	BU	**PSI**	**PSI**	**PSI**
log $p(CO_2)$/bar	-2.88	-2.81	-2.11	-2.35
pH	7.37	7.37	7.04	7.20
pe	-2.90	-3.17	-2.73	-3.00
Eh	-0.172	-0.187	-0.161	-0.177
IS /m	n.d.	0.509	0.151	1.007
Molality				
Al	n.d.	2.05E-08	2.10E-08	2.14E-08
Ba	n.d.	1.81E-07	9.90E-08	3.97E-07
C(IV)	9.96E-04	1.02E-03	2.15E-03	2.29E-03
Ca	2.90E-02	2.90E-02	2.02E-02	2.03E-02
Cl	0.407	0.407	0.078	0.924
F	1.25E-04	1.71E-04	1.55E-04	2.12E-04
Fe	**1.15E-04**	**9.08E-06**	3.07E-05	1.99E-05
K	2.73E-03	2.74E-03	2.13E-03	2.13E-03
Mg	1.99E-02	1.89E-02	1.45E-02	1.45E-02
Mn	n.d.	1.07E-04	8.46E-05	6.61E-05
Na	0.366	0.368	0.054	0.900
S(VI)	2.98E-02	2.98E-02	2.28E-02	2.34E-02
Si	9.10E-05	1.68E-04	1.77E-04	1.53E-04
Sr	2.68E-04	4.19E-04	2.39E-04	8.64E-04

4.3 Calculation of Bentonite Pore Waters (BPW)

The results of the BPW calculations obtained by reaction of 0.1141 kg of the six formerly defined OPAw (PSI variants) with 1 kg bentonite clay are shown and compared with the corresponding reacting OPAw in the next two tables.

Tab. 4-3 shows the results obtained through reaction of MX-80 Na-bentonite with the three OPAw from NL-ZNO. The water denoted BPW_NL-ZNO-22 is defined as the reference bentonite pore water for the calculation of solubility limits and sorption coefficients of dose-relevant radionuclides, to be used in safety assessment calculations. In various Nagra reports, this water is called E3-BPW-Ref (Curti et al. 2023, Curti 2022, Johnson et al. 2023, Hummel et al 2023). Like the reference BPW defined for SGT-2, it is in equilibrium with a pCO_2 of $10^{-2.2}$ bar. The other two variants define a low pH and a high pH BPW corresponding to the proposed limiting values of pCO_2 in the Opalinus Clay formation ($10^{-2.8}$ and $10^{-1.8}$ bar). The BPW with high CO_2-contents ($pCO2 = 10^{-1.8}$ bar) is referred to as E3-BPW_highpCO2 in Nagra publications (Hummel et al., 2023). Tab. 4-4 lists the BPW results obtained from reaction of bentonite with the revised Bülach OPAw (called E3-BPW_sal in Nagra documentations) and with the two artificial waters presented in the preceding Section.

The reaction and buffering mechanisms discussed in Chapter 3 are confirmed in these final BPW calculations. Specifically, a slight pH increase is observed compared to the reacting OPAw, except for the artificial high-salinity water, in which case a slight decrease from pH 7.20 to 6.97 is computed. Overall, the new calculations yield, as expected, a narrow pH-range (7.0 – 7.5) similar to that defined by the sensitivity analysis in the model-testing calculations.

Moreover, siderite is again found to be unstable, as the initial MX-80 inventory is dissolved completely in all six calculations and the dissolved Fe is converted to magnetite and pyrite. Together with the narrow pH range, the pyrite-magnetite equilibrium constrains the system to a narrow range of reducing oxidation potentials (Eh = -194 to -157 mV) similar to that determined in the test cases.

It must be noted here that for the present final BPW calculations it was no longer necessary to suppress goethite from the assemblage of potentially precipitating solids. In all six calculations goethite precipitation was allowed, however (contrary to the test calculations) in no case precipitation occurred. This is a consequence of the revised thermodynamic data for this phase in TDB2020, which indicate that the former data were not appropriate and led to an exceedingly high stability of goethite (Hummel & Thoenen 2022).

Tab. 4-3: Upper section: in-situ bentonite pore waters (BPW) for the NL-ZNO region compared to the reacting Opalinus Clay Waters (OPAw)

Lower section: initial and final amounts (at equilibrium) of exchanged cations and minor solids in MX-80 bentonite. All calculations were carried out at 25 °C, 1 bar.

Description	**Low pCO_2**		**Reference BPW**		**High pCO_2**	
Calc. ID	OPAw_NL-ZNO-28	**BPW_NL-ZNO-28**	OPAw_NL-ZNO-22	**BPW_NL-ZNO-22**	OPAw_NL-ZNO-18	**BPW_NL-ZNO-18**
Nagra ID		**E3-BPW-lowpCO2**		**E3-BPW-Ref**		**E3-BPW_highpCO2**
log $p(CO_2)$/bar	-2.79	-2.80	**-2.20**	**-2.20**	-1.80	-1.80
pH	7.40	7.51	**7.10**	**7.24**	6.90	7.05
pe	-3.22	-3.29	**-2.83**	**-2.94**	-2.58	-2.70
Eh	-0.190	-0.194	**-0.167**	**-0.173**	-0.152	-0.159
IS /m	0.317	0.452	**0.319**	**0.452**	0.321	0.453
Aqueous concentrations [mol/kgw]						
Al	2.13E-08	2.45E-08	**2.09E-08**	**2.08E-08**	2.86E-08	2.39E-08
Ba	1.56E-07	7.84E-08	**1.57E-07**	**7.19E-08**	1.58E-07	6.85E-08
C(IV)	1.07E-03	1.37E-03	**2.21E-03**	**2.94E-03**	3.68E-03	4.99E-03
Ca	2.01E-02	1.92E-02	**2.03E-02**	**1.77E-02**	2.05E-02	1.69E-02
Cl	0.239	0.238	**0.240**	**0.239**	0.241	0.240
F	1.74E-04	1.74E-04	**1.74E-04**	**1.74E-04**	1.74E-04	1.74E-04
Fe	7.14E-06	6.42E-06	**2.56E-05**	**2.09E-05**	5.95E-05	4.65E-05
K	2.13E-03	1.92E-03	**2.13E-03**	**1.83E-03**	2.14E-03	1.79E-03
Mg	1.43E-02	1.12E-02	**1.45E-02**	**1.02E-02**	1.46E-02	9.77E-03
Mn	8.16E-05	1.82E-05	**8.24E-05**	**1.84E-05**	8.33E-05	1.86E-05
Na	0.215	0.391	**0.215**	**0.375**	0.216	0.366
S(VI)	2.29E-02	7.16E-02	**2.29E-02**	**7.86E-02**	2.29E-02	8.29E-02
Si	1.73E-04	1.70E-04	**1.72E-04**	**1.70E-04**	1.72E-04	1.70E-04
Sr	3.67E-04	1.87E-04	**3.70E-04**	**1.72E-04**	3.73E-04	1.64E-04
Exch. [mol/kg clay]	*Initial*	*Final*	***Initial***	***Final***	*Initial*	*Final*
BaZ_2	5.00E-04	1.56E-07	**5.00E-04**	**1.53E-07**	5.00E-04	1.52E-07
CaZ_2	3.30E-02	3.68E-02	**3.30E-02**	**3.62E-02**	3.30E-02	3.58E-02
KZ	1.30E-02	1.30E-02	**1.30E-02**	**1.30E-02**	1.30E-02	1.30E-02
MgZ_2	2.00E-02	1.95E-02	**2.00E-02**	**1.91E-02**	2.00E-02	1.89E-02
NaZ	6.68E-01	6.66E-01	**6.68E-01**	**6.68E-01**	6.68E-01	6.69E-01
SrZ_2	2.00E-03	3.74E-04	**2.00E-03**	**3.68E-04**	2.00E-03	3.64E-04

Tab. 4-3: Cont.

Description Calc. ID	**Low pCO_2**		**Reference BPW**		**High pCO_2**	
	OPAw_NL-ZNO-28	**BPW_NL-ZNO-28**	**OPAw_NL-ZNO-22**	**BPW_NL-ZNO-22**	**OPAw_NL-ZNO-18**	**BPW_NL-ZNO-18**
Nagra ID		**E3-BPW-lowpCO2**		**E3-BPW-Ref**		**E3-BPW_highpCO2**
Solids [mol/kg clay]	*Initial*	*Final*	***Initial***	***Final***	*Initial*	*Final*
Barite	0	5.00E-04	**0**	**5.00E-04**	0	5.00E-04
Calcite	3.00E-01	3.11E-01	**3.00E-01**	**3.12E-01**	3.00E-01	3.13E-01
Dolomite	0	9.04E-04	**0**	**1.36E-03**	0	1.63E-03
Pyrite	5.00E-01	5.04E-01	**5.00E-01**	**5.04E-01**	5.00E-01	5.04E-01
Celestine	0	1.65E-03	**1.00E-12**	**1.66E-03**	0	1.66E-03
Kaolinite	3.90E-02	3.90E-02	**3.90E-02**	**3.90E-02**	3.90E-02	3.90E-02
Gypsum	2.35E-02	7.95E-03	**2.35E-02**	**7.14E-03**	2.35E-02	6.64E-03
Siderite	8.60E-02	0	**8.60E-02**	**0**	8.60E-02	0
Magnetite	4.30E-01	4.57E-01	**4.30E-01**	**4.57E-01**	4.30E-01	4.57E-01
Quartz	1.66E+00	1.66E+00	**1.66E+00**	**1.66E+00**	1.66E+00	1.66E+00
Rhodochrosite	0	7.23E-06	**0**	**7.30E-06**	0	7.37E-06
Fluorite	0	0	**0**	**0**	0	0

Tab. 4-4: Upper section: in-situ Bülach bentonite pore water (BPW_BUL-28) compared to the reacting OPAw and artificial low-salinity and high-salinity BPWs

Lower section: initial and final amounts (at equilibrium) of exchanged cations and minor solids in MX-80 bentonite. All calculations were carried out at 25 °C, 1 bar.

Description Calc. ID	**Bülach water**		**Low salinity water**		**High salinity water**	
	OPAw_BUL -28	**BPW_BUL-28**	OPAw_NL-ZNO-ls	**BPW_NL-ZNO-ls**	OPAw_NL-ZNO-hs	**BPW_NL-ZNO-hs**
Nagra ID		E3-BPW_sal				
log $p(CO_2)$/bar	-2.81	-2.80	-2.11	-2.20	-2.35	-2.21
pH	7.37	7.42	7.04	7.33	7.20	6.97
pe	-3.17	-3.20	-2.73	-3.03	-3.00	-2.66
Eh	-0.187	-0.189	-0.161	-0.179	-0.177	-0.157
IS /m	0.509	0.592	0.151	0.353	1.007	1.084
Aqueous concentrations [mol/kgw]						
Al	2.05E-08	2.21E-08	2.10E-08	2.07E-08	2.14E-08	1.90E-08
Ba	1.81E-07	1.13E-07	9.90E-08	5.12E-08	3.97E-07	2.38E-07
C(IV)	1.02E-03	1.19E-03	2.15E-03	3.48E-03	2.29E-03	2.00E-03
Ca	2.90E-02	2.71E-02	2.02E-02	1.29E-02	2.03E-02	5.40E-02
Cl	0.407	0.405	0.078	0.078	0.924	0.922
F	1.71E-04	1.70E-04	1.55E-04	1.54E-04	2.12E-04	1.65E-04
Fe	9.08E-06	8.49E-06	3.07E-05	1.64E-05	1.99E-05	5.35E-05
K	2.74E-03	2.41E-03	2.13E-03	1.44E-03	2.13E-03	3.89E-03
Mg	1.89E-02	1.56E-02	1.45E-02	7.45E-03	1.45E-02	2.98E-02
Mn	1.07E-04	1.83E-05	8.46E-05	1.82E-05	6.61E-05	1.90E-05
Na	0.368	0.496	0.054	0.289	0.900	0.845
S(VI)	2.98E-02	5.91E-02	2.28E-02	1.02E-01	2.34E-02	4.54E-02
Si	1.68E-04	1.66E-04	1.77E-04	1.74E-04	1.53E-04	1.53E-04
Sr	4.19E-04	1.87E-04	2.39E-04	1.25E-04	3.73E-04	1.64E-04
Exch. [mol/kg clay]	*Initial*	*Final*	***Initial***	***Final***	*Initial*	*Final*
BaZ_2	5.00E-04	1.47E-07	5.00E-04	1.66E-07	5.00E-04	1.15E-07
CaZ_2	3.30E-02	3.50E-02	3.30E-02	3.89E-02	3.30E-02	2.83E-02
KZ	1.30E-02	1.30E-02	1.30E-02	1.31E-02	1.30E-02	1.28E-02
MgZ_2	2.00E-02	1.85E-02	2.00E-02	2.06E-02	2.00E-02	1.50E-02
NaZ	6.68E-01	6.71E-01	6.68E-01	6.59E-01	6.68E-01	6.92E-01
SrZ_2	2.00E-03	3.52E-04	2.00E-03	3.99E-04	2.00E-03	2.75E-04

Tab. 4-4: Cont.

Description Calc. ID	**Bülach water**		**Low salinity water**		**High salinity water**	
	OPAw_BUL -28	**BPW_BUL-28**	OPAw_NL-ZNO-ls	**BPW_NL-ZNO-ls**	OPAw_NL-ZNO-hs	**BPW_NL-ZNO-hs**
Nagra ID		E3-BPW_sal				
Solids [mol/kg clay]	*Initial*	*Final*	***Initial***	***Final***	*Initial*	*Final*
Barite	0	5.00E-04	0	5.00E-04	0	5.00E-04
Calcite	3.00E-01	3.10E-01	3.00E-01	3.14E-01	3.00E-01	3.10E-01
Dolomite	0	1.87E-03	0	2.21E-04	0	3.29E-03
Pyrite	5.00E-01	5.04E-01	5.00E-01	5.04E-01	5.00E-01	5.04E-01
Celestine	0	1.67E-03	0	1.61E-03	0	1.76E-03
Kaolinite	3.90E-02	3.90E-02	3.90E-02	3.90E-02	3.90E-02	3.90E-02
Gypsum	2.35E-02	1.02E-02	2.35E-02	4.52E-03	2.35E-02	1.09E-02
Siderite	8.60E-02	0	8.60E-02	0	8.60E-02	0
Magnetite	4.30E-01	4.57E-01	4.30E-01	4.57E-01	4.30E-01	4.57E-01
Quartz	1.66E+00	1.66E+00	1.66E+00	1.66E+00	1.66E+00	1.66E+00
Rhodochrosite	0	1.01E-05	0	7.57E-06	0	5.38E-06
Fluorite	0	0	0	0	0	2.66E-06

5 Acknowledgments

Many thanks are due to Dmitrii Kulik and Dan Miron for their valuable technical support in setting up the GEM-Selektor model and its transfer to TDB2020. I am grateful to Wolfgang Hummel for his careful review of the report.

6 References

Arvidson R.S. & MacKanzie F.T. (1999): The dolomite problem: control of precipitation kinetics by temperature and saturation state. American Journal of Science 299, 257-288

Berner U., Kulik D.A. & Kosakowski G. (2013): Geochemical impact of a low-pH cement liner on the near field of a repository for spent fuel and high-level radioactive waste. Physics and Chemistry of the Earth 64, 46-56

Birgersson M. & Karnland O. (2009): Ion equilibrium between montmorillonite interlayer space and an external solution – consequences for diffusional transport. Geochim. Cosmochim. Acta 73, 1908-1923

Birgersson M. (2017): A general framework for ion equilibrium calculations in compacted bentonite. Geochim. Cosmochim. Acta 200, 186-200

Birgerrson et al. (2017): Bentonite buffer: macroscopic performance from nanoscale properties; Chapter 12, Section 12.2.5.1 in: Michael J. Apted and Joonhong Ahn, eds., Geological Repository Systems for Safe Disposal of Spent Nuclear Fuels and Radioactive Waste, Elsevier

Blanc P., Lassin A., Piantone P., Azaroual M., Jacquemet N., Fabbri A. & Gaucher E. C. (2012): Thermoddem: A geochemical database focused on low temperature water/rock interactions and waste materials: Applied Geochemistry 27, 2107-2116

Bradbury M.H. & Baeyens B. (2002): Porewater chemistry in compacted re-saturated MX-80 bentonite: Physico-chemical characterisation and geochemical modelling. PSI Bericht 02-10, Paul Scherrer Institut, Villigen, Switzerland

Bradbury M.H., Berner U., Curti E., Hummel W., Kosakowski G. & Thoenen T. (2014): The Long Term Geochemical Evolution of the Nearfield of the HLW Repository. Nagra Technical Report NTB 12-01

Cudennec Y. & Lecerf A. (2006): The transformation of ferrihydrite into goethite or hematite, revisited. J. Solid State Chem. 179, 716-722

Curti E. (1993): Modelling bentonite pore waters for the Swiss high-level radioactive waste repository. PSI-Bericht 93-05, Paul Scherrer Institut, Villigen, Switzerland

Curti E. & Wersin P. (2002): Assessment of Porewater Chemistry in the Bentonite Backfill for the Swiss SF/HLW Repository. Nagra Technical Report NTB 02-09

Curti, E. (2022): Aqueous corrosion of vitrified nuclear waste: Current process understanding, literature review and recommended rates. Nagra Arbeitsbericht NAB 23-09

Curti, E., Thoenen, T., Miron, D., Bayens, B., Van Loon, L. & O.X. Leupin (2023): The chemical near-field evolution within a HLW/SF repository section. Nagra Technical Report NTB 22-06

Gimmi Th. & Alt-Epping P. (2018): Simulating Donnan equilibria based on the Nernst-Planck equation. Geochim. Cosmochim. Acta 232, 1-13

Grenthe I., Plyasunov A. V. & Spahiu K. (1997): Estimations of Medium Effects on Thermodynamic Data. In: Modelling in Aquatic Chemistry, Grenthe I. and Puigdomènech I., Eds., Nuclear Energy Agency, Organisation for Economic Co-operation and Development (OECD), Paris, France, pp. 325-426

Grenthe I., Mompean F., Spahiu K. & Wanner H. (2013): Guidelines for the extrapolation to zero ionic strength, Version of 18 June 2013, OECD Nuclear Energy Agency, Data Bank, Issy-les-Moulineaux (France)

Hadi, J., Wersin, P., Jenni, A., & Greneche, J.M. (2017): Redox evolution and Fe-bentonite interaction in the ABM2 experiment, Äspö Hard Rock Laboratory. Nagra Technical Report NTB 17-10

Hadi J., Wersin P., Serneels V. & Greneche J.-M. (2019): Eighteen years of steel–bentonite interaction in the FEBEX in situ test at the Grimsel test site in Switzerland. Clays and Clay Minerals, 67(2), 111-131

Hummel, W. & Thoenen, T. (2022): The PSI Chemical Thermodynamic Database 2020. Nagra Technical Report NTB 21-03

Hummel, W., Kulik, D.A. & Miron G.D (2023) Solubility limits for bentonite near field (update of NTB 14-06). Nagra Technical Report NTB 23-04

Jenni A., Wersin P., Thoenen T., Baeyens B., Ferrari A., Gimmi T., Mäder U., Marschall P., Hummel W. & Leupin O. (2019): Bentonite backfill performance in a high-level waste repository: a geochemical perspective. Technical Report NTB 19-03

Johnson, L.H., Curti, E. & Spahiu, K. (2023) : A radionuclide release model for spent UO2 and MOX fuel for safety assessment with application to waste to be disposed of in a deep geological repository in Switzerland. Nagra Arbeitsbericht NAB 23-10

Kinniburgh D.G. & Cooper D.M. (2004): Predominance and Mineral Stability Diagrams Revisited, Environ. Sci. Technol. 38, 3641-3648

Kittrick J.A. & Peryea F.J. (1988): Experimental Validation of the Monophase Structure Model for Montmorillonite Solubility. Soil Sci. Soc. Am. J. 52, 1199-1201

Kulik D.A., Wagner T., Dmytrieva S.V., Kosakowski G., Hingerl F.F., Chudnenko K.V., Berner, U. (2013): GEM-Selektor geochemical modeling package: revised algorithm and GEMS3K numerical kernel for coupled simulation codes. Computational Geosciences 17, 1-24

Kulik D.A., Fernandes M.M. & Baeyens B. (2018): The 2SPNE SC/CE sorption model in GEM-Selektor v.3.4 code package (ClaySor): Implementation, tests, and user guide. Nagra Arbeitsbericht NAB 18-27

Mäder U. (2009): Reference pore water for the Opalinus Clay and “Brown Dogger” for the provisional safety-analysis in the framework of the sectoral plan (SGT-ZE). Nagra Arbeitsericht NAB 09-14

Mäder, U. & Wersin, P. (2022): Porewater composition in Opalinus Clay. Nagra Arbeitsbericht NAB 22-47

May H.M., Kinniburgh D.G., Helmke P.A. & Jackson M.L. (1986): Aqueous dissolution, solubilities and thermodynamic stabilities of common alumosilicate clay minerals: kaolinite and smectites. Geochim. Cosmochim. Acta 50(8), 1667-1677

Müller-Vonmoos M. & Kahr G. (1983): Mineralogische Untersuchungen von Wyoming Bentonite MX-80 und Montigel. Nagra Technischer Bericht NTB 83-13

Roberts J., Kenwarda P.A., Fowle D.A., Goldstein R.H., Gonzalez L.A. & Moore D.S. (2013): Surface chemistry allows for abiotic precipitation of dolomite at low temperature. PNAS, 14540-14545

Schwertmann U., Stanjek H. & Becher H.H. (2004): Long-term in vitro transformation of 2-line ferrihydrite to goethite/hematite at 4, 10, 15 and 25 °C. Clay Minerals 39, 433-438

Thoenen T., Hummel W., Berner U. & Curti E. (2014): The PSI/Nagra Chemical Thermodynamic Database 12/07. PSI-Report 14-04, Paul Scherrer Institut, Villigen, Switzerland

Tournassat C., Bourg I. C., Holmboe M., Sposito G. & Steefel C.I. (2016): Molecular dynamics simulations of anion exclusion in clay interlayer nanopores. Clays Clay Miner. 64, 374-388

Wersin P., Curti E. & Appelo C.A.J. (2004): Modelling bentonite–water interactions at high solid/liquid ratios: swelling and diffuse double layer effects. Applied Clay Sci. 26, 249- 257

App. A List of SIT coefficients used in BPW calculations

Tab. A-1: Selected SIT coefficients for BPW chemical modelling

Missing or unreliable experimental values have been estimated according to the procedure described in Hummel & Thoenen (2022), Section 1.5.3.

j	k	ε(j,k)
Al(SO4)+	Cl-	0.05
Al(SO4)2-	Na+	-0.05
Al+3	Cl-	0.33
AlF+2	Cl-	0.15
AlF2+	Cl-	0.05
AlF3@	Cl-	0
AlF4-	Na+	-0.05
AlF5-2	Na+	-0.1
AlF6-3	Na+	-0.15
AlO+	Cl-	0.05
AlO2-	Cl-	-0.05
AlO2H@	Cl-	0
AlOH+2	Cl-	0.15
AlHSiO3+2	Cl-	0.15
AlSiO5-3	Na+	-0.15
Ba(CO3)@	Cl-	0
Ba(HCO3)+	Cl-	0.05
Ba(SO4)@	Cl-	0
Ba+2	Cl-	0.07
BaOH+	Cl-	0.05
Ca(CO3)@	Cl-	0
Ca(HCO3)+	Cl-	0.05
Ca(SO4)@	Cl-	0
Ca+2	Cl-	0.14
CaF+	Cl-	0.1
CaOH+	Cl-	0.05
Ca(HSiO3)+	Cl-	0.05
CaSiO3@	Cl-	0

Tab. A-1: Cont.

j	k	ε(j,k)
Cl-	Na+	0.03
Fe(CO3)@	Cl-	-0.05
Fe(HCO3)+	Cl-	0
Fe(HSO4)+	Cl-	0.05
Fe(SO4)@	Cl-	0
Fe+2	Cl-	0.17
FeCl+	Cl-	0.16
FeF+	Cl-	0.05
FeOH+	Cl-	0.05
Fe(HSO4)+2	Cl-	0.58
Fe(SO4)+	Cl-	0.4
Fe(SO4)2-	Na+	0.24
Fe+3	Cl-	0.76
Fe2(OH)2+4	Cl-	1
Fe3(OH)4+5	Cl-	1
FeCl+2	Cl-	0.64
FeCl2+	Cl-	0.52
FeCl3@	Cl-	0
FeF+2	Cl-	0.4
FeF2+	Cl-	0.2
FeF3@	Cl-	0
FeO+	Cl-	0.43
FeO2-	Na+	-0.05
FeO2H@	Cl-	0
FeOH+2	Cl-	0.27
FeHSiO3+2	Cl-	0.04
K(SO4)-	Na+	-0.05
K+	Cl-	0
KOH@	Cl-	0
Mg(CO3)@	Cl-	0
Mg(HCO3)+	Cl-	0.05
Mg+2	Cl-	0.19
MgF+	Cl-	-0.02
MgOH+	Cl-	0.05

Tab. A-1: Cont.

j	k	ε(j,k)
MgSO4@	Cl-	0
Mg(HSiO3)+	Cl-	0.05
MgSiO3@	Cl-	0
Na+	Cl-	0.03
Na(CO3)-	Na+	-0.05
Na(HCO3)@	Cl-	0
Na(SO4)-	Na+	-0.05
NaF@	Cl-	0
NaOH@	Cl-	0
HSiO3-	Na+	-0.05
Si4O10-4	Na+	0
SiO2@	Cl-	0
SiO3-2	Na+	-0.07
Sr(CO3)@	Cl-	0
Sr(HCO3)+	Cl-	0.05
Sr(SO4)@	Cl-	0
Sr+2	Cl-	0.12
SrOH+	Cl-	0.05
CO2@	Cl-	0
CO3-2	Na+	-0.08
HCO3-	Na+	0
CH4@	Cl-	0
ClO4-	Na+	0.01
H2@	Cl-	0
N2@	Cl-	0
O2@	Cl-	0
S2O3-2	Na+	-0.08
HSO3-	Na+	-0.01
SO3-2	Na+	-0.08
HSO4-	Na+	-0.01
SO4-2	Na+	-0.12
H2S@	Cl-	0
HS-	Na+	-0.05
S-2	Na+	-0.1

Tab. A-1: Cont.

j	k	ε(j,k)
OH-	Na+	0.04
H+	Cl-	0.12
H2O@	Cl-	0

App. B Conversion of Gaines-Thomas to Vanselow selectivity coefficients

We start by defining the equivalent fraction E_i and mole fraction X_i of an exchanged cation i in an exchanger containing K different cations

$$E_i \equiv \frac{z_i\, n_i}{\sum_{k=1}^{K}(z_k\, n_k)}\,,\; X_i \equiv \frac{n_i}{\sum_{k=1}^{K}(n_k)} \tag{A2-1}$$

where K is the total number of exchanging species, n_i, n_k are mole amounts and z_i, z_k the charges of cations i, k, respectively. For exchange between divalent Ca^{2+} and monovalent Na^{+} on exchange site = Y, the following reaction can be defined:

$$2\ NaY + Ca^{2+} = CaY_2 + 2\ Na^{+}$$

The Gaines-Thomas (K_G) and Vanselow (K_V) selectivity coefficients for the preceding reaction are defined as:

$$K_G \equiv \frac{E_{Ca}\, a_{Na}^2}{E_{Na}^2\, a_{Ca}} \tag{A2-2}$$

$$K_V \equiv \frac{X_{Ca}\, a_{Na}^2}{X_{Na}^2\, a_{Ca}} \tag{A2-3}$$

where a_i, E_i and X_i denote the aqueous activity, equivalent fraction and mole fraction of the cation i on the clay, respectively. Combining (A2-2) and (A2-3) the aqueous activities cancel out, yielding:

$$K_V \equiv K_G\, \frac{X_{Ca}\, E_{Na}^2}{X_{Na}^2\, E_{Ca}} \tag{A2-4}$$

For a generic bi-ionic exchange reaction

$$z_B A Y_{zA} + z_A B^{zB+} = z_A B Y_{zB} + z_B A^{zA+}$$

describing exchange between ions A, B with charges z_A and z_B one obtains:

$$K_V \equiv K_G\, \frac{X_B^{z_A}\, E_A^{z_B}}{X_A^{z_B}\, E_B^{z_A}} \;=\; K_G \left(\frac{E_A}{X_A}\right)^{z_B} \left(\frac{X_B}{E_B}\right)^{Z_A} \tag{A2-5}$$

Further, after defining:

$$X_B \equiv x \rightarrow X_A = 1 - x \tag{A2-6a}$$

$$E_B \equiv e \rightarrow E_A = 1 - e \tag{A2-6b}$$

the following relation between *e* and *x* can be derived:

$$e = \frac{2x}{x+1} \tag{A2-7a}$$

$$x = \frac{e}{2-e} \tag{A2-7b}$$

where *x* and *e* are the mole and equivalent fractions of the divalent ion B, respectively.

Equation (A2-5) can be now expressed in terms of *x* and *e*:

$$K_V = K_G \left(\frac{1-\frac{2x}{x+1}}{1-x}\right)^2 \left(\frac{x}{\frac{2x}{x+1}}\right) = K_G \left(\frac{1}{1+x}\right)^2 \frac{(1+x)}{2} = K_G \frac{1}{2(1+x)} \tag{A2-8a}$$

$$K_V = K_G \left(\frac{1-e}{1-\frac{e}{2-e}}\right)^2 \left(\frac{\frac{e}{2-e}}{e}\right) = K_G \left(\frac{(1-e)(2-e)}{2\,(1-e)}\right)^2 \frac{1}{2-e} = K_G \frac{2-e}{4} \tag{A2-8b}$$

The above equations allows the transformation of K_G to K_V (or vice versa) for a bi-ionic system at any specific equivalent fraction or mole fraction for a monovalent-divalent exchange reaction. This result shows that there is no "one to one" correspondence between Gaines-Thomas and Vanselow constant, as the value of the latter depends on the specific distribution of exchanged ions (and vice-versa). Therefore, a conversion from K_G to K_V is only possible when the equivalent fraction determined at equilibrium in the experiment(s) used to determine K_G is known.

Eqs. (A2-8a,b) can be easily generalized for any pair of charges in a bi-ionic exchange reaction. Starting again from eq. (A2-5) and defining the ratio of the charges of the exchanging cations as $R = z_A/z_B$, one obtains after algebraic transformations:

$$e = \frac{x}{x+R(1-x)} \tag{A2-9a}$$

$$x = \frac{eR}{e(R-1)+1} \tag{A2-9b}$$

Inserting these results again into eq. (A2-5) and defining the right-hand sides of (A2-9a,b) as $e(x) \equiv \beta$ and $x(e) \equiv \alpha$ we obtain:

$$K_V = K_G \left(\frac{1-e}{1-\alpha}\right)^{z_B} \left(\frac{\alpha}{e}\right)^{Z_A} \quad \text{(A10-a)}$$

$$K_V = K_G \left(\frac{1-\beta}{1-x}\right)^{z_B} \left(\frac{x}{\beta}\right)^{Z_A} \quad \text{(A10-b)}$$

These equations were solved in a spreadsheet, yielding the plot shown in Fig. B-1. The plots shows, for the indicated exchanged ion pairs, the ratio of Gaines-Thomas to Vanselow selectivity coefficients as a function of the equivalent fraction of the higher charged cation.

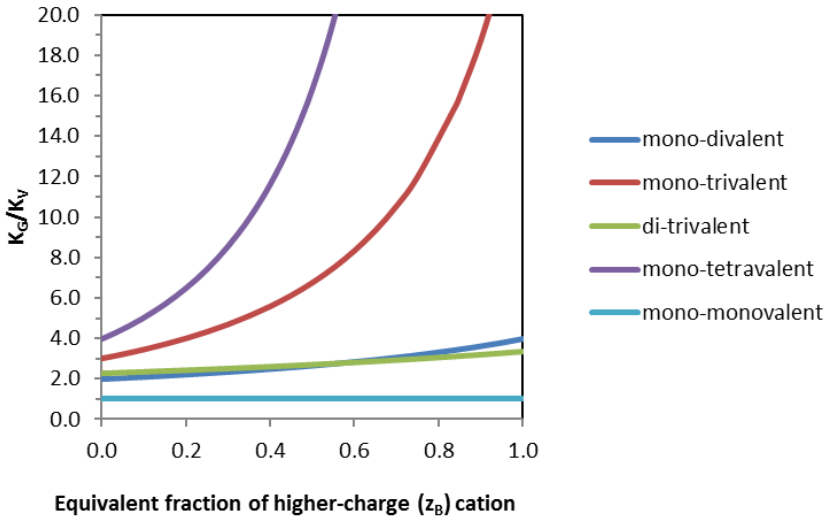

Fig. B-1: Ratio of Gaines-Thomas to Vanselow constant as a function of equivalent fraction and charge of the exchanging cations (binary system)

Tab. B-1 reports the Vanselow coefficients used in the SGT3 BPW model, after transformation from the Gaines-Thomas coefficients and equivalent fractions data reported by Bradbury & Baeyens (2002) for experimentally characterized MX-80 bentonite. Na-Sr and Na-Ba coefficients were approximated based on information available in the cited reference.

Tab. B-1: Transformation of Gaines-Thomas to Vanselow selectivity coefficients from eq. (A2-8b) for Na^+-K^+, Na^+-Mg^{2+}, Na^+-Ca^{2+}, Na^+-Sr^{2+} and Na^+-Ba^{2+} exchange reactions

Original data from Tab. A8 in Bradbury & Baeyens (2002) are given in blue.

	meq/kg	**Equivalent fraction**	K_G	**log** K_G	K_V	**log** K_V
CEC	**787**					
Na	668	0.849	-	-	-	-
K	13	0.017	4.0	0.602	4.000	0.602
Mg	40	0.051	2.2	0.342	1.072	0.030
Ca	66	0.084	2.6	0.415	1.245	0.095
Sr	3.935	0.005	2.6	0.415	1.297	0.113
Ba	1	0.001	2.6	0.415	1.299	0.114

App. C Explanation of discrepant Fe concentrations in calculated Opalinus Clay waters

The recalculation of the Uni-Bern Opalinus Clay pore waters with GEM-Selektor v. 3.9.0 and the updated thermodynamic database (TDB 2020) yielded in general only minor differences in pH, ionic strength, pe and elemental concentrations. The only exception were Fe concentrations, which in some cases are by one order of magnitude lower than in the original version, supplied by Bern University and computed with PHREEQC using version 12/07 of the PSI-Nagra database. Because the iron data have been thoroughly reviewed (based on the extensive, recent NEA reviews) and many data updated, it is possible that the different computed Fe concentrations arise from differences in specific thermodynamic Fe data.

To check this hypothesis, we recalculated the GEM-Selektor version of OPAw_ZNO-28 (the calculation showing the largest discrepancy in Fe concentrations) using GEM-Selektor v. 3.7.0 with PSI-Nagra TDB 12/07. Ideally, such a calculation would reproduce more closely the higher Fe concentration ($[Fe]_{tot} = 8.65 \times 10^{-5}$ mol/kgw) computed in the original PHREEQC version. A comparison of the essential results is shown in Tab. C-1.

Tab. C-1: Comparison of results obtained for the low pCO_2 variant of the ZNO Opalinus Clay pore water

Calc. ID	**OPAw_ZNO-28**	**OPAw_ZNO-28**	**OPAw_ZNO-28**
Implementor **Code** **Database**	**BU** **PHREEQC** **TDB 12/07**	**PSI** **GEMS 3.9.0** **TDB 2020**	**PSI** **GEMS 3.7.0** **TDB 12/07**
log $p(CO_2)$/bar	-2.80	-2.79	-2.81
pH	7.40	7.40	7.41
pe	-3.00	-3.22	-3.10
Eh	-0.178	-0.190	-0.182
IS /m	0.312	0.317	0.318
Molality			
Al	1.41E-08	2.13E-08	1.58E-08
Ba	1.56E-07	1.56E-07	1.82E-07
C(IV)	1.02E-03	1.07E-03	1.07E-03
Ca	2.01E-02	2.01E-02	2.03E-02
Cl	0.240	0.239	0.239
F	1.33E-04	1.74E-04	1.40E-04
Fe	**8.45E-05**	**7.14E-06**	**1.00E-05**
K	2.13E-03	2.13E-03	2.13E-03
Mg	1.53E-02	1.43E-02	1.51E-02
Na	0.213	0.215	0.215

Tab. C-1: Cont.

Calc. ID	**OPAw_ZNO-28**	**OPAw_ZNO-28**	**OPAw_ZNO-28**
Implementor **Code** **Database**	**BU** **PHREEQC** **TDB 12/07**	**PSI** **GEMS 3.9.0** **TDB 2020**	**PSI** **GEMS 3.7.0** **TDB 12/07**
S(VI)	2.29E-02	2.29E-02	2.42E-02
Si	1.78E-04	1.73E-04	1.79E-04
Sr	2.70E-04	3.67E-04	3.19E-04

The GEM-Selektor recalculation with TDB 12/07 leads to only slightly higher Fe concentrations. The difference to the PHREEQC version calculated with the same data is still more than a factor of 8. Therefore, the discrepancy must be due to other reasons.

A key result of the GEM-Selektor calculation is that siderite, which is set in the input file as a solubility controlling solid with an inventory of 0.1 mmoles, is in all cases dissolved, leading to precipitation of magnetite. The assemblage controlling Fe concentrations is then always pyrite + magnetite. Increasing the amount of siderite to avoid its complete dissolution, leads then to the ternary equilibrium assemblage pyrite + magnetite + siderite. This corresponds to a pseudo-invariant point analogous to that represented in the Eh-pH diagram of Fig. 3-1c. Eh and pH are then fixed to values that are different and inconsistent with those obtained in the GEM-Selektor calculations shown in Tab. C-1. Obviously, it is not possible to adjust pH and Eh as long as all three minerals are stable. Other test calculations with GEM-Selektor showed that it is not possible for the system to reach equilibrium at pH 7.4 and Eh in the range -180/-190 mV assuming siderite + pyrite equilibrium.

In the PHREEQC calculation, the stable assemblage is however just siderite + pyrite. To resolve this apparent inconsistency, we checked the saturation indices for the controlling Fe minerals in the two calculations (Tab. C-2). It turns out that (logically) siderite is undersaturated (i.e. unstable) in the GEM-Selektor calculations and saturated in the PHREEQC calculation. Pyrite is saturated (i.e. stable) in all three calculations. Magnetite is saturated (stable) in the GEM-Selektor calculations, but turns out to be strongly oversaturated in the PHREEQC calculation. Indeed, magnetite (or any other Fe^{3+} oxide) was not specified explicitly in the selection of minerals required to be saturated in the PHREEQC input file (keyword "EQUILIBRIUM_PHASES). In such cases PHREEQC allows the solution to remain metastable with respect to all unspecified solids.

Tab. C-2: Comparison of saturation indices of iron minerals in three variants of the Opalinus Clay pore water OPAw-ZNO-28

Calc. ID	**OPAw_ZNO-28**	**OPAw_ZNO-28**	**OPAw_ZNO-28**
Implementor **Code** **Database**	**BU** **PHREEQC** **TDB 12/07**	**PSI** **GEMS 3.9.0** **TDB 2020**	**PSI** **GEMS 3.7.0** **TDB 12/07**
Saturation index			
Pyrite	0.0	0.0	0.0
Siderite	0.0	**-1.1**	**-0.9**
Magnetite	**+2.9**	0.0	0.0

In the BPW calculations, magnetite (the major corrosion product of anaerobic steel corrosion) and other Fe- oxides (e.g. goethite, ferrihydrite) are retained as potentially precipitating phases. For consistency reasons, they are included as possible equilibrium phases also in the Opalinus Clay pore waters (there is no reason to exclude them). Therefore, the lower calculated Fe concentrations calculated with GEM-Selektor were accepted.